

August 2014

The Development of VDR-coactivator Inhibitors and Their Evaluation Using Biochemical and Cell-based Assays

Belaynesh Feleke

University of Wisconsin-Milwaukee

Follow this and additional works at: <https://dc.uwm.edu/etd>

 Part of the [Chemistry Commons](#)

Recommended Citation

Feleke, Belaynesh, "The Development of VDR-coactivator Inhibitors and Their Evaluation Using Biochemical and Cell-based Assays" (2014). *Theses and Dissertations*. 526.
<https://dc.uwm.edu/etd/526>

This Thesis is brought to you for free and open access by UWM Digital Commons. It has been accepted for inclusion in Theses and Dissertations by an authorized administrator of UWM Digital Commons. For more information, please contact open-access@uwm.edu.

THE DEVELOPMENT OF VDR-COACTIVATOR INHIBITORS
AND THEIR EVALUATION USING BIOCHEMICAL AND
CELL-BASED ASSAYS

by

Belaynesh D Feleke

A Thesis Submitted in

Partial Fulfillment of

Requirements for the Degree of

Master of Science

in Chemistry

at

The University of Wisconsin-Milwaukee

August 2014

ABSTRACT

THE DEVELOPMENT OF VDR-COACTIVATOR INHIBITORS AND THEIR EVALUATION USING BIOCHEMICAL AND CELL-BASED ASSAYS

by

Belaynesh D Feleke

The University of Wisconsin-Milwaukee, 2014

Under the Supervision of Professor Alexander Arnold, PhD

The vitamin D receptor (VDR) belongs to the family of nuclear receptors and plays a crucial role in many biological processes such as cell differentiation, cell proliferation and calcium homeostasis. VDR is a good pharmaceutical target for many diseases including cancer, metabolic disorders, skin diseases and cardiovascular diseases. Upon binding with its endogenous ligand calcitriol in the body, VDR undergoes a conformational change that disrupts the interaction with corepressor proteins and instead enables the interaction with coactivator proteins that mediated transcription. The goal of the research is the development of new small molecules that will selectively inhibit the interaction between VDR and coregulators by binding to the ligand binding site of VDR.

Eleven VDR antagonists were synthesized based on GW0742 a potent PPAR δ agonist that inhibit VDR-mediated transcription at higher concentrations. The compounds were evaluated using cell-based and biochemical assays to determine their ability to inhibit the interaction between VDR and steroid receptor coactivator-2 (SRC-2) and to determine

the ability to activate PPAR δ mediated transcription. BF040813F and BF090813A1 were the most active compounds towards VDR without activating PPAR δ . The simple accessibility of BF040813F, being a precursor compound, makes it an attractive candidate for further SAR studies.

© Copyright by Belaynesh D Feleke, 2014
All Rights Reserved

ACKNOWLEDGEMENTS

I would like to thank my advisor Dr. Alexander “Leggy” Arnold for his patience, encouragement, and guidance. He is the best advisor anyone could wish for.

I would also like to thank Dr. Nick Silvaggi and Dr. Peng for serving on my master’s committee.

Additionally, I would like to thank my husband Jacob Zewdie and my good Friends Ezana Mekonen, Nardos Gizaw, Habtamu Bedasso and anyone who helped me through graduate school, including people in my research group.

TABLE OF CONTENTS

	Page
LIST OF FIGURES	X
LIST OF TABLES	XIII
LIST OF ABBREVIATIONS	XIV
CHAPTER I	1
1. Introduction	1
1.1 1, 25-Dihydroxyvitamin D ₃	2
2.2 VDR-mediated transcription.....	4
1.3 VDR Antagonist.....	6
CHAPTER II	7
2. Synthesis of new VDR antagonists	7
2.1. Introduction.....	7
2.2. New proposed VDR antagonists	8
2.3. Synthesis of proposed new VDR antagonists	9
2.3.1. Synthesis of 4-substituted VDR antagonists.....	9
2.3.2. Synthesis of 3-substituted VDR antagonists.....	11

2.3.3. Synthesis of 5-substituted VDR antagonists.....	12
2.4. Experimental section.....	14
CHAPTER III	22
3. Assays to evaluate VDR antagonists	22
3.1. Luminescence and detection	22
3.2 Fluorescence polarization and detection	25
3.3. The VDR-Coregulator FP assay	27
3.4 The VDR-mediated transcription assay	29
3.5 Toxicity assay	31
3.6 Experimental procedures	32
3.6.1. Protocol to determine the interaction between VDR and coregulator SRC2- 3.....	32
3.6.2. Protocol to determine the VDR-mediated inhibition of transcription	32
3.6.3. Protocol to determine the PPAR α -mediated inhibition of transcription....	36
3.6.4 Protocol to determine the viability of cells	37
CHAPTER IV.....	38
4. Summary of results	38
4.1 BF050813G.....	38
4.2 BF040813F	39

4.3	BF060813H.....	40
4.4	BF090713B.....	41
4.5	BF090613C.....	42
4.6	BF090813A.....	44
4.7	BF090712D.....	45
4.8	BF090713B1.....	46
4.9	BF090613C1.....	47
4.10	BF090813A1.....	48
4.11	F090812E.....	49
CHAPTER V.....		51
5.	Discussion and conclusions.....	51
CHAPTER VI.....		54
1.	Summary of data.....	54
CHAPTER VII.....		57
¹H-NMR and ¹³C-NMR.....		57
	Compound 1.2.....	58
	Compound 1.3.....	59
	Compound BF040813F.....	60

Compound BF090613C	62
Compound BF090812E	64
Compound BF090712D	66
Compound 2.2.....	67
Compound 2.3.....	69
Compound BF050813G	70
Compound BF090713B	71
Compound 3.2.....	75
Compound 3.3.....	76
Compound BF060813H	78
Compound BF090813A	79
Compound BF090813A1	81
CHAPTER VIII	83
References.....	83

LIST OF FIGURES

Figure 1: General structure of nuclear receptor	2
Figure 2. Chemical structure of 1, 25-(OH) ₂ D ₃	3
Figure 3: Vitamin D formation and metabolism.....	3
Figure 4: VDR-retinoid x receptor dimer in the absence of ligand.	4
Figure 5: Binding of a ligand enables VDR to perform transcription	5
Figure 6: Structure of compound GW 0742.	7
Figure 7: Different parts of the GW0742 molecule that were modified.....	8
Figure 8: New proposed VDR antagonists	9
Figure 9: Synthesis of compound 1.6	10
Figure 10: Synthesis of compound 2.6.	12
Figure 11: Synthesis of compound 3.6.	14
Figure 12: Schematic diagram depicting the generation of light from luminescent molecules in the excited state	23
Figure 13: Luminometer detection system.	24
Figure 14: Fluorescence Polarization Assay principle [31].....	26
Figure 15: Fluorescence detection	27
Figure 16: Cartoon of fluorescent polarization assay used to screen inhibitors	27

Figure 17: LG190178: Synthetic Agonist for Vitamin D Receptor.....	29
Figure 18: 24OH luciferase plasmid vector [36]	30
Figure 19: Enzymatic reaction of luciferase.	31
Figure 20: Summary of BF050813G; A) FP; B) VDR-mediated transcription (antagonist mode); C) Toxicity; D) PPAR δ -mediated transcription (agonist mode)	39
Figure 21: Summary of BF040813F; A) FP; B) VDR-mediated transcription (antagonist mode); C) toxicity; D) PPAR δ -mediated transcription (agonist mode)	40
Figure 22: Summary of BF060813H; A) FP; B) VDR-mediated transcription (antagonist mode); C) toxicity; D) PPAR δ -mediated transcription (agonist mode)	41
Figure 23: Summary of BF090713B; A) FP; B) VDR-mediated transcription (antagonist mode); C) toxicity; D) PPAR δ -mediated transcription (agonist mode)	42
Figure 24: Summary of BF090613C; A) FP; B) VDR-mediated transcription (antagonist mode); C) toxicity; D) PPAR δ -mediated transcription (agonist mode)	43
Figure 25: Summary of BF090613C; A) FP; B) VDR-mediated transcription (antagonist mode); C) toxicity; D) PPAR δ -mediated transcription (agonist mode)	44
Figure 26: Summary of BF090712D; A) FP; B) VDR-mediated transcription (antagonist mode); C) toxicity; D) PPAR δ -mediated transcription (agonist mode)	45
Figure 27: Summary of BF090613B1; A) FP; B) VDR-mediated transcription (antagonist mode); C) toxicity; D) PPAR δ -mediated transcription (agonist mode)	46

Figure 28: Summary of BF090613C1; A) FP; B) VDR-mediated transcription (antagonist mode); C) toxicity; D) PPAR δ -mediated transcription (agonist mode) 47

Figure 29: Summary of BF090613C1; A) FP; B) VDR-mediated transcription (antagonist mode); C) toxicity; D) PPAR δ -mediated transcription (agonist mode) 49

Figure 30: Summary of BF090613C1; A) FP; B) VDR-mediated transcription (antagonist mode); C) toxicity; D) PPAR δ -mediated transcription (agonist mode) 50

LIST OF TABLES

Table	Page
SUMMARY OF THE COMPOUNDS TESTED	52-53

LIST OF ABBREVIATIONS

AF: Activation Function

CMV: Cytomegalovirus

CBI: Coregulator binding inhibitor

DBD: DNA binding domain

DMSO: Dimethyl sulfoxide

DCM: Dichloromethane

FP: Fluorescence polarization

HTS: High-throughput screening

LBD: Ligand binding domain

LiAlH₄: Lithium aluminum hydride

N-CoR: Nuclear receptor corepressor

RE: Response element

SMART: Silencing mediator of retinoic acid and thyroid hormone

SRC: Steroid receptor coactivator

THF: Tetrahydrofuran

NR: Nuclear recepto

CHAPTER I

1. INTRODUCTION

The vitamin D receptor (VDR) is a transcription factor that belongs to the superfamily of 48 nuclear receptors (NRs). As a member of nuclear receptors, it mediates the transcription of genes responsible for cell differentiation, cell proliferation and calcium homeostasis.[1]

VDR is also pharmaceutical target for several diseases including, skin diseases, hyper-proliferative diseases, such as psoriasis, benign prostate hyperplasia, different types of cancer, autoimmune diseases, microbial infections, and osteoporosis.

Nuclear receptors generally share a common structural organization (**Figure 1**).[2]

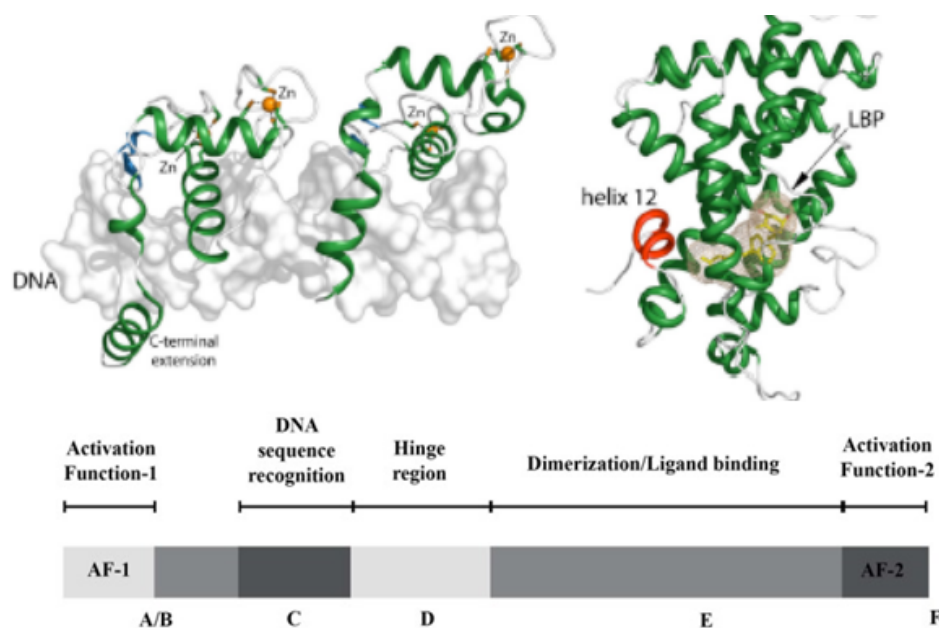


Figure 1: General structure of nuclear receptor

The N-terminal domain is highly variable depending on the receptor and contains a ligand-independent transactivation domain termed “Activation Function 1” (AF-1). The most conserved central region of the nuclear receptors is the DNA-binding domain (DBD) or the C domain, which is responsible for direct DNA interaction. Its main function is to recognize and bind specific DNA regulatory sites called response elements (REs). The flexible hinge, or D region, links the C-domain to the ligand-binding (E/F) domain. The ligand binding domain of nuclear receptors comprises the ligand binding pocket and also acts as a molecular switch by interpreting the ligand structure into conformational changes converting the receptor into an activator or repressor. The LBD remains the main feature that triggers biological responses to very diverse lipophilic molecules. The F domain is located at the end C-terminus of NRs. Because of its high variability in sequence, little is known about its structure and functional role.[3]

1.1 1, 25-Dihydroxyvitamin D3

The vitamin D hormone, 1, 25-dihydroxyvitamin D3 [1,25(OH)₂D₃], binds VDR with high affinity (**Figure 2**).[4]

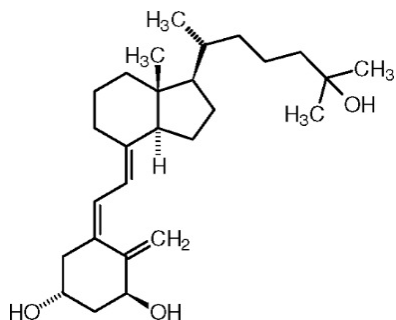


Figure 2. Chemical structure of 1, 25-(OH)₂D₃.

Its precursor, Vitamin D (**Figure 3**), can be obtained through foods we eat or can

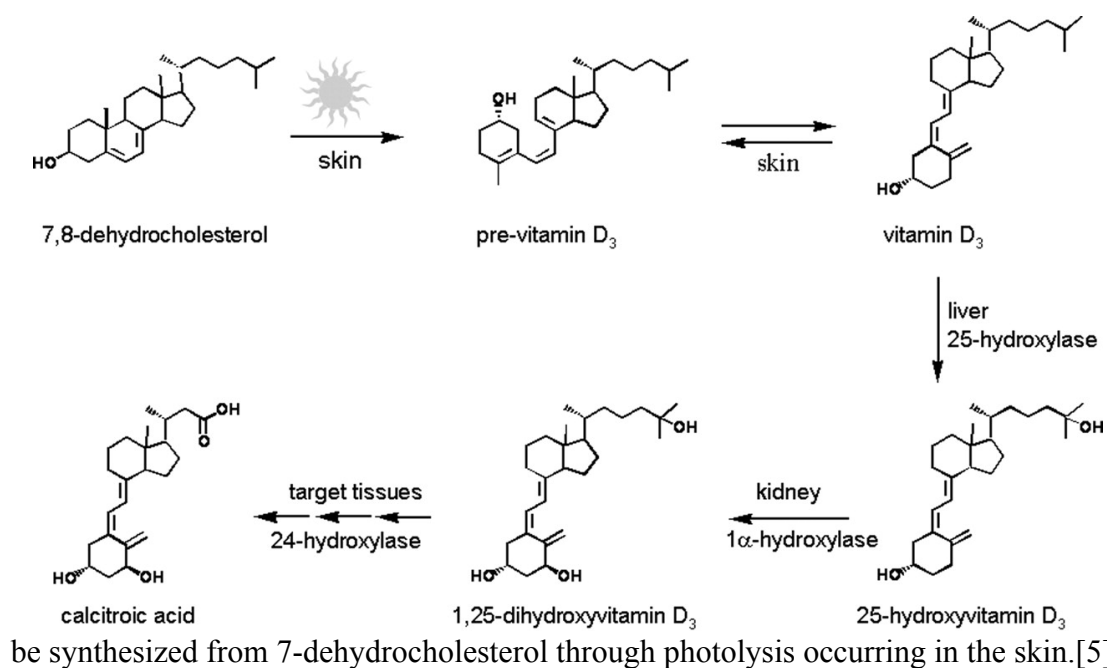


Figure 3: Vitamin D formation and metabolism. [6]

From there, the vitamin D binding protein shuttles vitamin D to the liver, where it is hydroxylated at carbon 25 by vitamin D 25-hydroxylase, resulting in the formation of 25-hydroxyvitamin D₃. [6] Vitamin D₃ then binds to its binding protein and is transported to the kidneys. In the kidneys, 25-hydroxyvitamin D₃ is then hydroxylated at carbon 1 of the A ring, which converts the vitamin D₃ to the active form, 1, 25-dihydroxyvitamin D₃. [7] Vitamin D₃ and its derivatives are metabolized in the presence of 24-hydroxylase to 24-hydroxylated products and eventually forming calcitric acid. [8, 9]

2.2 VDR-mediated transcription

In the nucleus, VDR binds DNA and forms a heterodimer with the retinoid X receptor (RXR) (Figure 4). [10]

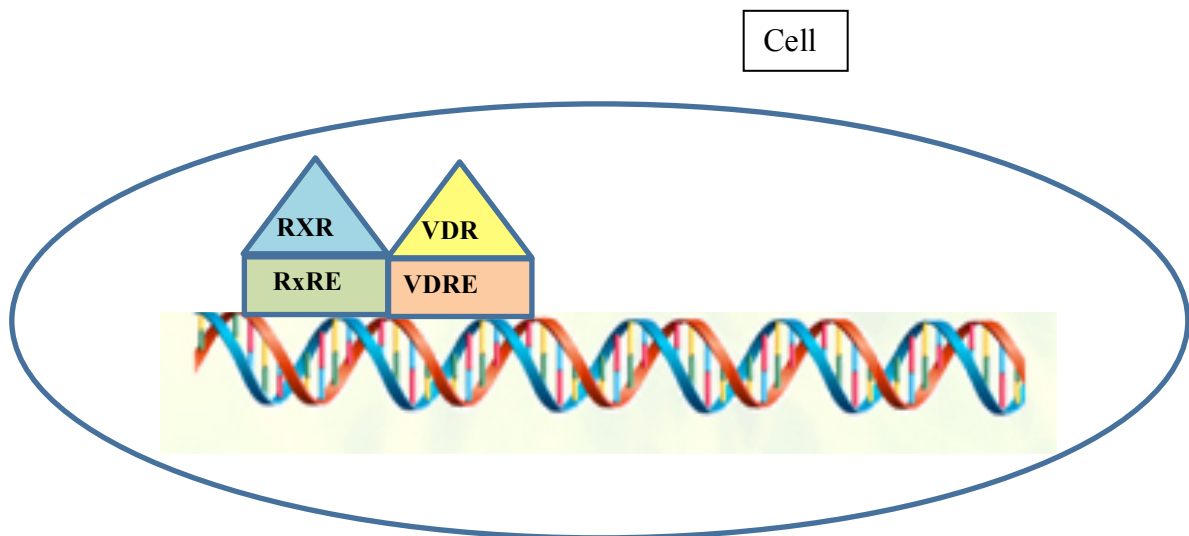


Figure 4: VDR-retinoid x receptor dimer in the absence of ligand.

RXR is also a nuclear receptor and binds 9-*cis* retinoic acid.[11] In the absence of the ligand, VDR is associated with corepressors such as the nuclear receptor corepressor (N-CoR) and the silencing mediator of retinoic acid and thyroid hormone receptor (SMRT).[12] N-CoR and SMRT are corepressor proteins that function to repress the transcriptional activity of VDR. Ligand binding, on the other hand, permits VDR-coactivator interactions, and allows the formation of multi-protein complexes that activate VDR-mediated transcription (**Figure 5**).

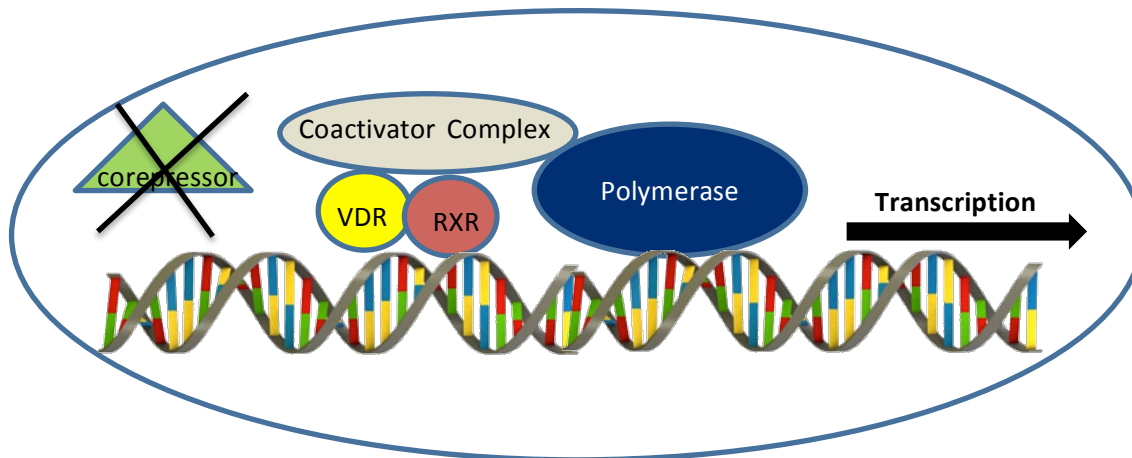


Figure 5: Binding of a ligand enables VDR to perform transcription

In the presence of 1, 25-(OH)₂ D₃, the VDR-LBD undergoes a conformational change which prevents corepressor binding and permits interactions with coactivator proteins such as steroid receptor coactivator 2, resulting in the formation of a multi-protein complex that activates VDR-mediated transcription. [13-15]

1.3 VDR Antagonist

VDR, as stated earlier, is a pharmaceutical target for different disorders including, cancer, skin disorder and autoimmune diseases. One way to modulate VDR-mediated transcription is the development of small molecules that inhibit the interactions between VDR and coregulators (corepressor and coactivators). Recently, VDR-coactivator inhibitors have been introduced by other groups and us.[16-19] The inhibition of VDR-coregulator interactions has shown to selectively modulate the expression of specific VDR genes. Most of the VDR antagonists developed are based on the secosteroidal scaffold, which is very hydrophobic and metabolically less stable. Our research presented herein, focuses on the introduction of non-secosteroidal VDR antagonists. These compounds have to be selective towards VDR without binding to other NRs.

CHAPTER II

2. SYNTHESIS OF NEW VDR ANTAGONISTS

2.1. Introduction

A HTS campaign in collaboration with NIH investigating 390000 molecules led to the identification of GW0742 (**Figure 6**) as a competitive VDR antagonist.[24]

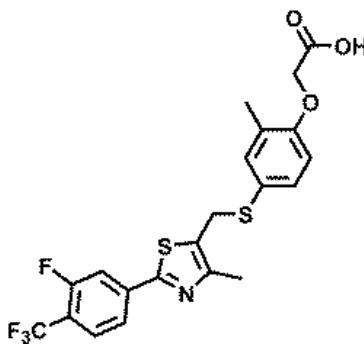


Figure 6: Structure of compound GW 0742.

GW0742 was introduced by GlaxoSmithKline in 2003 as a highly selective agonist for PPAR δ . [25] Since then, compound GW0742 has been investigated in cell-based assays and *in vivo*, in order to understand the role of PPAR δ in hypertension, diabetes, inflammation, obesity, and cancer [26, 27]. Research by other groups and us has shown that GW0742 inhibited the transcription of the VDR target gene, *CYP24A1*, in the presence of 1,25-(OH) $_2$ D $_3$. [28] It was determined that at micro molar concentrations GW0742 behaved as an antagonist of VDR. [24]

2.2. New proposed VDR antagonists

The approach for generating new selective and potent VDR antagonists involved the variation of different parts of the GW0742 molecule (**Figure 7**).

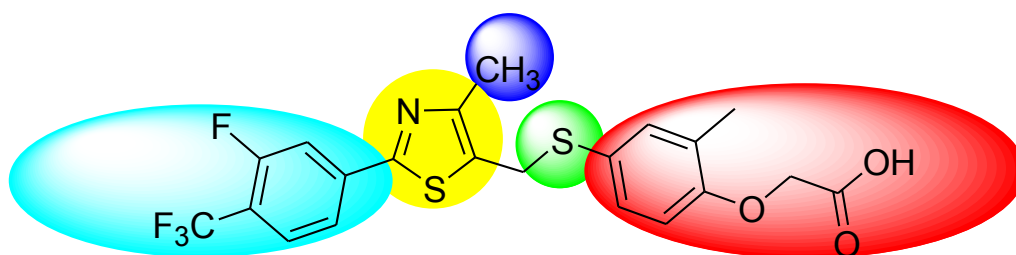


Figure 7: Different parts of the GW0742 molecule that were modified

The variation of the turquoise aryl moiety was carried out in collaboration with the NIH. The analysis of the compounds and their corresponding potency towards VDR antagonism and selectivity among nuclear receptors identified 2- and 3-methoxy as well as 2- and 3-trifluoromethyl substituents as superior among 87 compounds tested. With this in mind, we concentrated on the substitution of the thiazole moiety (yellow) with an aryl ring system and concentrated on the connectivity between the two moieties as depicted in **Figure 8**.

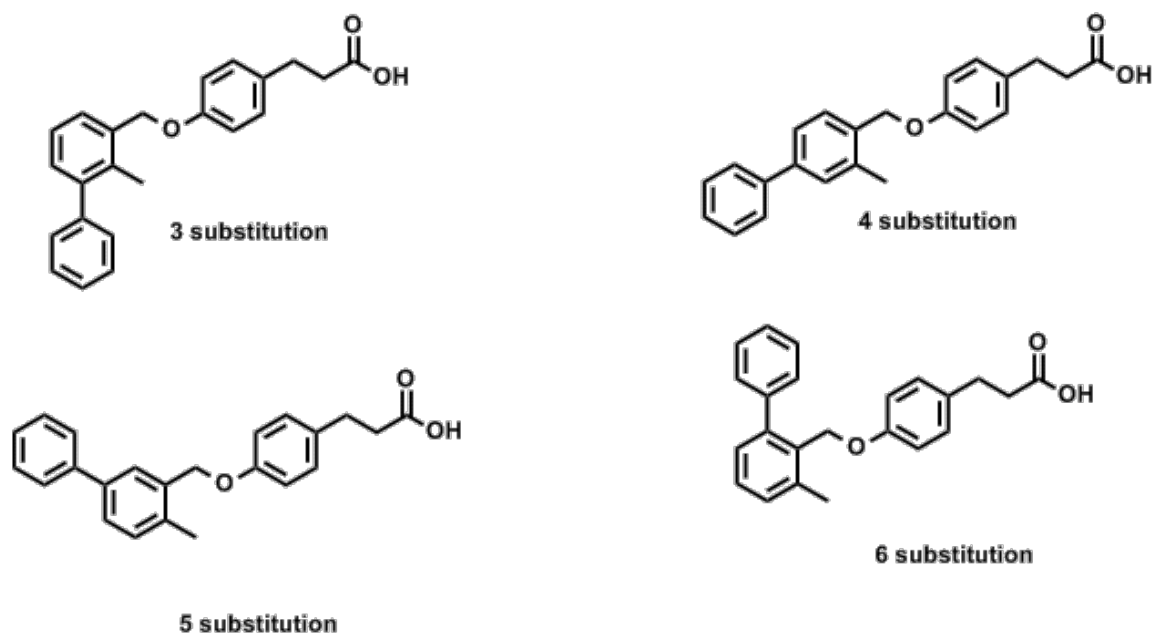


Figure 8: New proposed VDR antagonists

The different connectivity of the proposed VDR antagonists introduces a range of different angles. Our hypothesis is that this change will not only influence the affinity of these compounds towards VDR but also change the selectivity towards other nuclear receptors. Furthermore, we will introduce different substituents especially 2- and 3-methoxy as well as 2- and 3-trifluoromethyl substituents to optimize their potency.

2.3. Synthesis of proposed new VDR antagonists

2.3.1. Synthesis of 4-substituted VDR antagonists

The first step of the synthesis of the 4-substituted VDR antagonists started with the reduction of the carboxylic acid **1.1** to make the alcohol **1.2** was realized in the presence of lithium aluminum hydride at 0°C in THF (**Scheme 1**). After a reaction time of 6 hours the reaction was quenched with 1M HCl and the corresponding product was isolated in a yield of 51%.

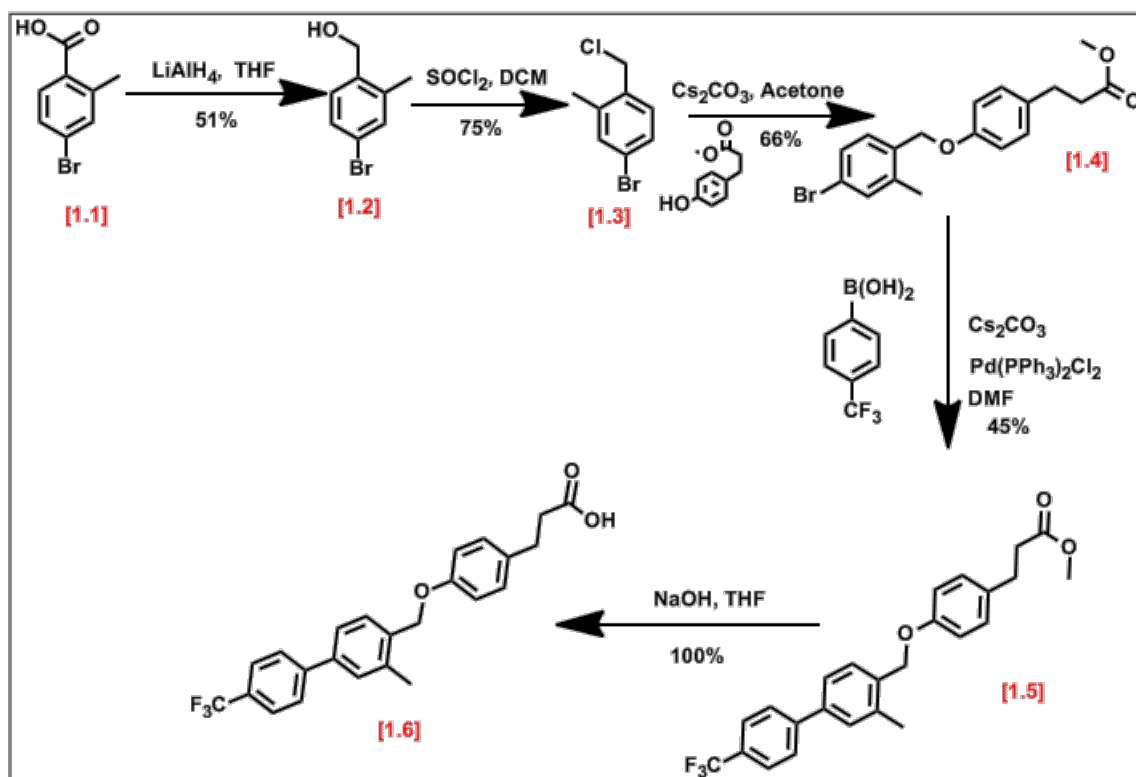


Figure 9: Synthesis of compound 1.6

The chloride **1.3** was formed with **1.2** in the presence of thionyl chloride. The excess of SOCl_2 was evaporated after 3 hours followed by evaporation at high vacuum overnight giving **1.3** in 75% yield. The reduction of **1.1** in the presence of LiAlH_4 also

formed 2-methyl benzyl alcohol, which was separated by a high vacuum step from the product by leaving it under high vacuum overnight. The chloride **1.3** is then coupled with the phenol in the presence of Cs_2CO_3 to form the ester **1.4** in 66%. The product is purified using column chromatography using a solvent gradient from 32% to 60% ethyl acetate in hexanes. Suzuki coupling reaction was then used to form **1.4** with 4-(Trifluoromethyl) phenyl boronic acid in the presence of $\text{Pd}(\text{PPh}_3)_2\text{Cl}_2$ to form **1.5** which is further hydrolyzed to the carboxylic acid final product **1.6**.

2.3.2. Synthesis of 3-substituted VDR antagonists

The next analogue synthesis of the 3-substituted VDR antagonists started with the reduction of the carboxylic acid **2.1** to make the alcohol **2.2** in the presence of lithium aluminum hydride at 0°C in THF (**Scheme 2**). After a reaction time of 6 hours the reaction was quenched with 1M HCl and the corresponding product was isolated in a yield of 51%. The chloride **2.3** was formed with **2.2** in the presence of thionyl chloride. The excess of SOCl_2 was evaporated after 3 hours followed by evaporation at high vacuum overnight giving **2.3** in 75% yield. The chloride **2.3** is then coupled with the phenol in the presence of Cs_2CO_3 to form the ester **2.4** in 66% yield. The product is purified using column chromatography using a solvent gradient from 32% to 60% ethyl acetate in hexanes. Suzuki coupling reaction was then used to form **2.4** with 2 methyl

methoxy phenyl boronic acid in the presence of $\text{Pd}(\text{PPh}_3)_2\text{Cl}_2$ to form **2.5**. The ester was further hydrolyzed to an acid in the presence of 8M NaOH to give **1.6**.

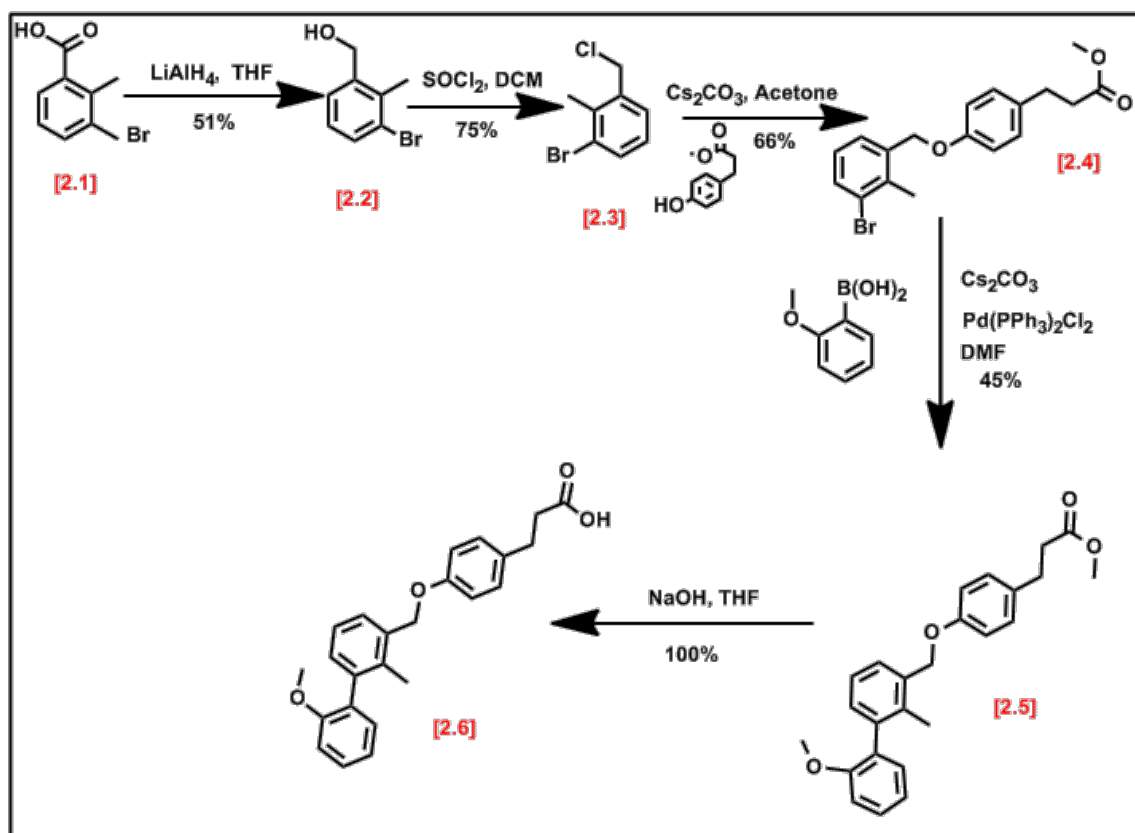


Figure 10: Synthesis of compound 2.6.

2.3.3. Synthesis of 5-substituted VDR antagonists

The next step of the synthesis of the 5-substituted VDR antagonists started with the reduction of the carboxylic acid **3.1** to make the alcohol **3.2** in the presence of lithium aluminum hydride at 0°C in THF (**Scheme 3**). After a reaction time of 6 hours the reaction was quenched with 1M HCl and the corresponding product was isolated in a yield of 51%. The chloride **3.3** was formed with **3.2** in the presence of thionyl chloride. The excess of SOCl₂ was evaporated after 3 hours followed by evaporation at high vacuum overnight giving **3.3** in 75% yield. The chloride **3.3** is then coupled with the phenol in the presence of Cs₂CO₃ to form the ester **3.4** in 66%. The product is purified using column chromatography using a solvent gradient from 32% to 60% ethyl acetate in hexanes. Suzuki coupling reaction was then used to form **3.4** with 4-(Trifluoromethyl) phenyl boronic acid in the presence of Pd(PPh₃)₂Cl₂ to form **3.5** which is further hydrolyzed to the carboxylic acid final product **3.6**.

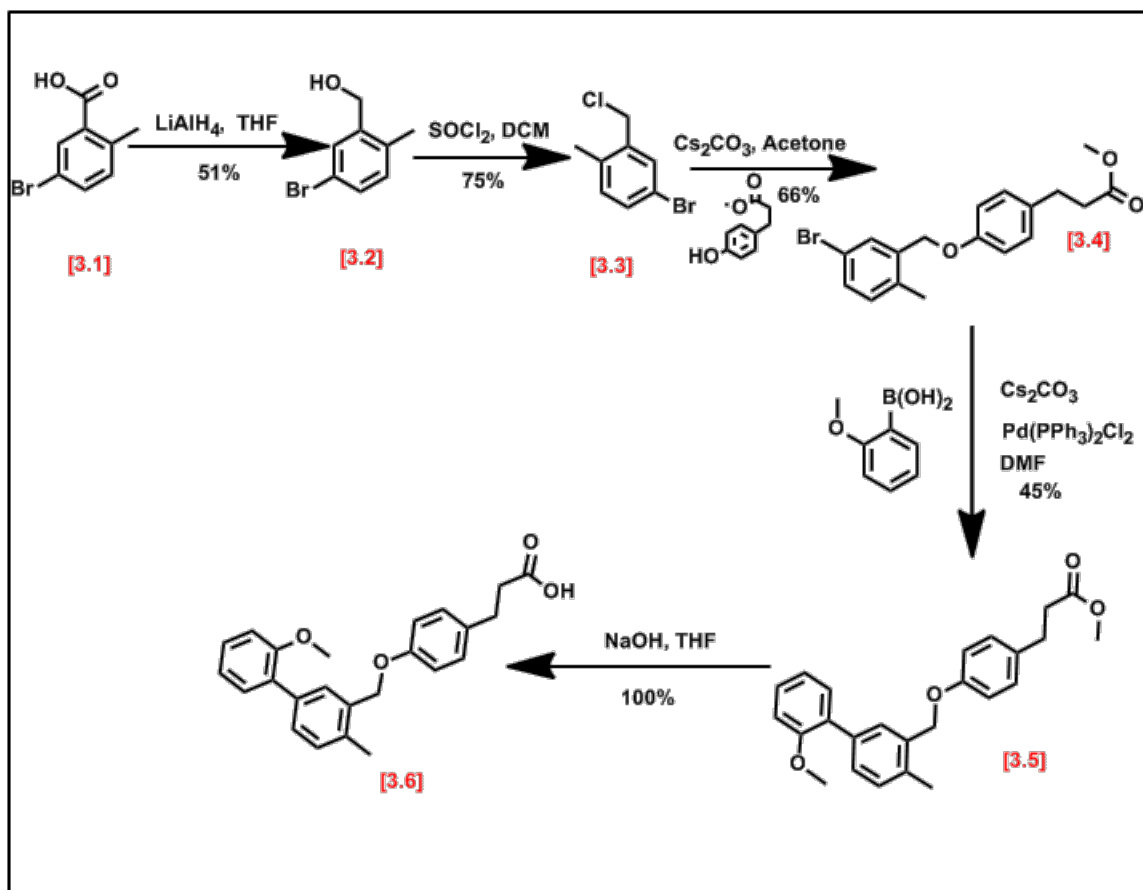
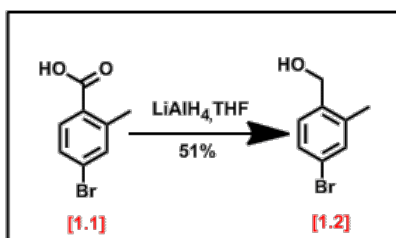


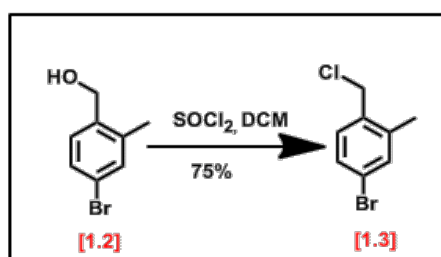
Figure 11: Synthesis of compound 3.6.

2.4. Experimental section

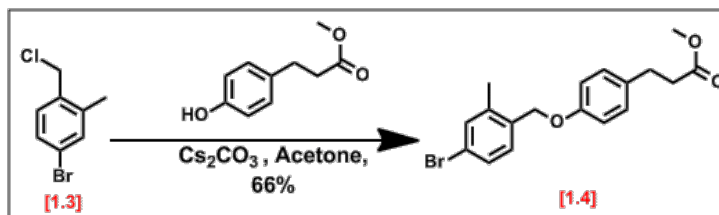
The carboxylic acid **1.1** (4.0g, 18.6mmol) in anhydrous THF (35mL) was added drop wise to LiAlH_4 (0.88g,



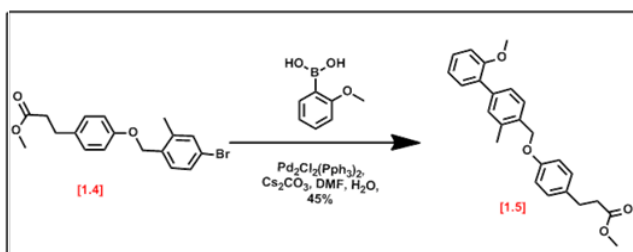
23.19mmol) in anhydrous THF (44mL) at 0°C over 30 minutes. The resulting mixture was slowly warmed to room temperature and stirred for 7 hours. The reaction was slowly quenched with water (300mL) acidified to PH<2. The mixture was worked up with DCM three times and was dried over Na₂SO₄. The organic layer was concentrated to give a white solid. The crude product **1.2** was left in the high vacuum over night and was used in the next step without purification. ¹HNMR (300MHz) (CDCl₃) δ 7.29(d, 1H); 7.14 (s, 1H); 7.12 (1H, d); 4.51 (s, 2H); 2.25 (s, 3H). ¹³C NMR δ 19.84, 25.52, 67.91, 130.37, 135.53, 136.83, 172.16.



The alcohol **2.2** (2g, 9.95mmol) was dissolved in Dichloromethane (4mL). Thionyl chloride (1.6mL) was slowly added drop wise to the above solution. The resulting mixture was stirred at room temperature for 24 hours. The organic solvent was removed using a rotary evaporator. The product **2.3** was then left under high vacuum overnight. ¹HNMR (300MHz) (CDCl₃) δ 7.38(d, 1H); 7.36 (s, 1H); 7.21 (d, 1H); 4.57 (s, 2H); 2.45 (s, 3H). From the ¹³C NMR the peak at δ 138.60, 133.78, 132.68, 130.47, 128.56, 121.94, 43.19, and 17.8 confirmed the formation of the chloride.



The crude benzyl chloride **1.3** (1.5g, 6.83mmol) and the phenol (1.5g, 8.33mmol) were dissolved in acetone (12mL) and treated with Cs_2CO_3 (0.6g). The reaction was stirred at 50°C for 16 hours. The reaction mixture was worked up with DCM three times and was dried over Na_2SO_4 . The organic layer was concentrated to give a white solid. The crude product **1.4** was purified by column chromatography with a solvent gradient from 32% to 60% ethyl acetate in hexanes. The fractions were concentrated to a white solid. ^1H NMR (300MHz) (CDCl_3) δ 7.39(s,1H,); 7.35 (1H,d, J=12);7.31 (d,1H,J=12); 7.17 (d,1H,J=9); 7.15(d, 1H, J=9); 6.94(d,1H, J=9); 6.91 (d,1H,J=9);4.96 (s,2H); 3.7 (s, 3H); 2.96-2.91 (t, 3H,J=6); 2.66-2.61 (t,2H J=6); 2.36, (s, 3H). ^{13}C NMR δ 173.15, 166.43, 148.95, 138.67, 137.11, 135.30, 130.87, 130.05, 129.08, 121.47, 119.28, 51.69, 35.63, 30.35, 19.75.

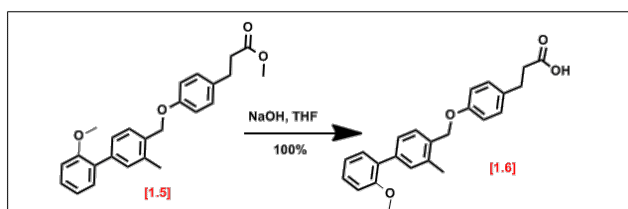


Commercially available 4-(Trifluoromethyl) phenyl boronic acid (100mg, mmol) and the ester **1.4** (51mg mmol) were suspended in DMF (4mL) and water (200 μL).

$\text{PdCl}_2(\text{pPh}_3)_2$ (10mg, mmol) was added followed by Cs_2CO_3 (292mg, mmol). The resulting mixture was stirred in the microwave at 160 °C for 10 min. The mixture was

acidified to $\text{pH} < 2$. The reaction was worked up with DCM three times and dried over Na_2SO_4 . The crude product **1.4** was purified by column chromatography with a gradient of 30% to 62% ethyl acetate in hexanes. The fractions were concentrated to a white solid. $^1\text{H NMR}$ (300MHz) (CDCl_3) δ 7.41-7.28(m, 6H); 7.06 (s,1H); 7.04 (d,1H, J=9); 7.02(d, 1H, J=9); 6.99(d,1H, J=9); 6.94 (d,1H,J=9); 5.04 (s,2H); 3.7 (s, 3H); 2.97-2.92 (t, 2H, J=6); 2.72-2.67 (t, 2H J=6); 2.44 (s, 3H). $^{13}\text{C NMR}$ δ 178.54, 157.62, 156.49, 138.59, 136.30, 133.51, 132.56, 131.56, 130.65, 129.26, 128.63, 128.41, 127.27, 120.80, 114.66,111.15, 68.56, 60.43, 55.51, 35.83, 29.04, 19.10.

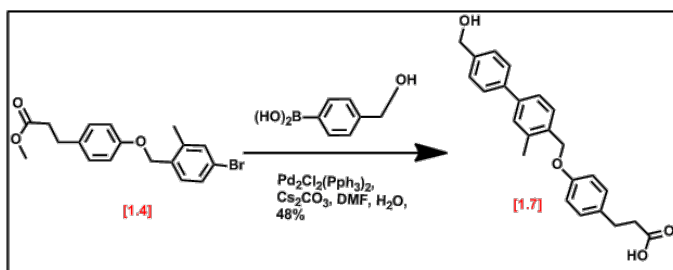
The ester **1.5** is hydrolyzed to the carboxylic acid form. **1.5** (20mg) of the ester was



dissolved in THF (1.5mL). 8M NaOH (0.15mL) was added and the resulting mixture was stirred over night at room

temperature. The mixture was acidified to $\text{pH} < 2$. The reaction was worked up with DCM three times and dried over Na_2SO_4 . The organic layer was concentrated to a white solid. $^1\text{H NMR}$ (300MHz) (CDCl_3) δ 7.41-7.28 (m, 6H); 7.19-7.16 (m,2H); 7.04 (d,1H,J=9); 7.02(d, 1H, J=9); 6.99(d,1H, J=9); 6.94 (d,1H,J=9);5.07 (s,2H); 3.83 (s,3H) ; 2.97-2.92 (t, 2H,J=6);2.72-2.67 (t, 2H J=6); 2.44 (s, 3H). $^{13}\text{C NMR}$ δ 176.22, 157.62, 156.49, 136.31, 133.51, 132.49, 131.56, 130.42, 130.85, 129.28, 128, 128.63, 127.26, 120.80, 114.86,111.15, 68.56, 55.53, 35.75, 29.52, 19.24.

Compound **1.7** was synthesized using the same procedure as compound **1.6**. A new



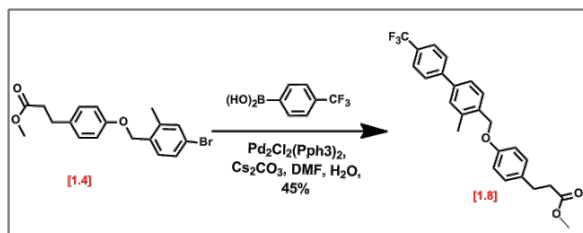
boronic acid was however used.

The hydroxyl group was found to be active on a HTS with the NIH.

Therefore (4-(hydroxymethyl)

phenyl) boronic acid was also used to couple with the **1.5** ester. Proton and Carbon NMR confirmed the formation of this acid. ^1H NMR (300MHz) (CDCl_3) δ 7.50 (s, 1H); 7.49 - 7.35 (m, 6H); 7.21 (d, 1H, J=9); 7.18(d, 1H, J=9); 6.98(d, 1H, J=9); 6.95 (d, 1H, J=9); 5.12 (s, 2H); 4.70 (s, 3H) ; 2.87-2.82 (t, 2H, J=6); 2.60-2.55 (t, 2H, J=6); 2.44 (s, 3H). ^{13}C NMR δ 173.42, 157.36, 137.38, 135.05, 133.08, 129.38, 129.27, 127.38, 225.73, 125.67, 124.92, 114.82, 68.27, 51.62, 35.98, 30.13, 19.08.

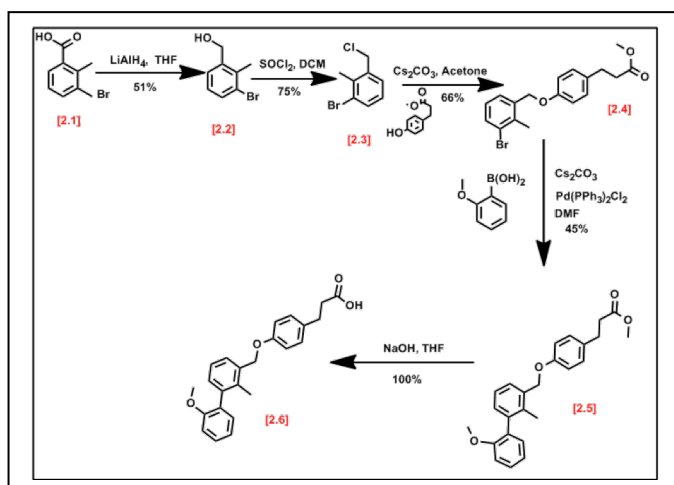
Compound **1.8** was also synthesized



the same way as compound **1.6** using a different boronic acid. The trifluoro group on the ring which was also on the GWO742 molecule and has shown

activity and hence was worth investigating. Therefore, 4-(Trifluoromethyl) phenyl)

boronic acid was also coupled with the ester compound to give **1.8**. ^1H NMR (300MHz) (CDCl_3) δ 7.7 (m, 4H); 7.55-7.48 (m, 3H); 7.19 (d, 1H, J=9); 7.16 (d, 1H, J=9); 6.96 (d, 1H, J=9); 6.95 (d, 1H, J=9); 5.09 (s, 2H); 3.7 (s, 3H); 2.97-2.92 (t, 2H, J=6); 2.67-2.64 (t, 2H, J=6); 2.48 (s, 3H). ^{13}C NMR δ 173.41, 157.35, 137.37, 135.06, 133.07, 129.33, 129.37, 129.27, 127.38, 225.71, 125.67, 124.92, 114.81, 68.20, 51.62, 35.97, 30.12, 19.08.



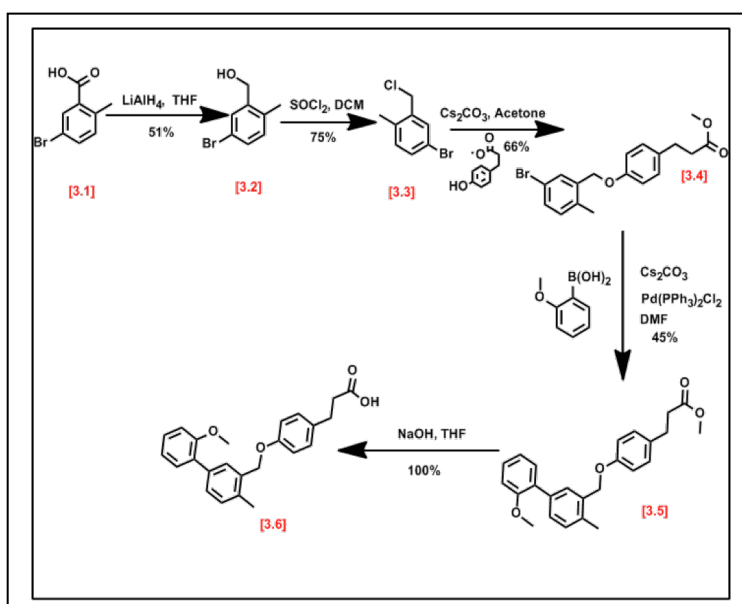
Reaction scheme 2 was performed the exact same way as reaction scheme 1. The corresponding NMR readings are as follows. **2.2**: ^1H NMR (300MHz) (CDCl_3) δ 7.52-7.00(m, 3H,); 4.6 (s, 2H); 2.35 (s, 3H). From the ^{13}C NMR the peak

at δ 61 confirmed the reduction to the alcohol. The crude NMR for **2.3** is as follows, ^1H NMR (300MHz) (CDCl_3) δ 7.59-7.04 (m, 3H,); 4.65 (s, 2H); 2.54 (s, 3H). From the ^{13}C NMR δ 139.80 135.01, 130.98, 129.91, 127.81, 125.65, 43.76, 19.93. Peak 43.7 confirmed the formation of the chloride. Pure NMR for **2.4** was ^1H NMR (300MHz) (CDCl_3) δ 7.41- 6.94(m, 7H); 5.04 (s, 2H); 3.7 (s, 3H); 2.98-2.93 (t, 2H, J=6); 2.69-2.64 (t, 2H, J=6); 2.48 (s, 3H). ^{13}C NMR δ 173.15, 157.43, 148.95, 138.67, 137.11, 135.30,

130.87, 129.05, 129.08, 118.60, 119.28, 68, 51.63, 35.97, 30.15, 18.73. NMR for **2.5**: ^1H NMR (300MHz) (CDCl_3) δ 7.42-6.97(m, 11H); 5.11 (2H,); 3.79 (s, 3H); 3.70 (s, 3H), 2.97-2.91(t, 3H, J=6 3H); 2.67-2.64 (t, 2H J=6); 2.06 (s, 3H). ^{13}C NMR δ 174.17, 158.27,157.38, 142.10, 136.27,135.51, 133.56, 131.87,130.95,129.98, 129.38, 128.52, 126.14, 121.19, 115.53, 111.35, 69.85, 56.12, 52.33, 36.71, 30.85, 16.45

For **2.6** ^1H NMR (300MHz) (CDCl_3) δ 7.3-6.9 (m, 11H); 5.11 (2H,); 3.7 (s, 3H); 2.98-2.93 (t, 2H, J=6); 2.72-2.67 (t, 2H J=6); 2.17 (s, 3H). ^{13}C NMR δ 178.52, 157.63,156.65, 139.38, 135.56, 134.79,132.48, 131.16 , 130.81, 130.25, 129.27, 129.05, 128.66, 128.66, 127.98, 125.43, 120.48, 114.92, 110.62, 69.15, 55.42, 35.79, 29.79, 16.45

Reaction scheme 3 was also performed using the same procedures as reaction



scheme 1 (**Figure 8**). The only difference being 5-bromo-2-methyl benzoic acid was used instead. The corresponding NMR readings are as follows. **3.2**: ^1H NMR (300MHz) (CDCl_3) δ 7.49(s, 1H,); 7.29-7.26 (d,

1H, J=9); 7.01-6.98 (d, 1H, J = 9). 4.6 (s, 2H); 2.21 (s, 3H). ¹³C NMR δ 141.64, 134.44, 131.40, 129.61, 127.27, 125.49, 119.08, 61.96, 17.39. The peak at 61 confirmed that the reduction had taken place. The crude NMR for **3.3** is as follows, ¹H NMR (300MHz) (CDCl₃) δ 7.49 (s, 1H); 7.48- 7.0 (m, 2H); 4.64 (s, 2H); 2.4 (s, 3H). ¹³C NMR δ 137.56, 136.08, 131.76, 129.82, 128.97, 119.53, 43.90, 18.35. From the ¹³C NMR, the peak around 43 confirmed the formation of the chloride. Pure NMR for **3.4** was ¹H NMR (300MHz) (CDCl₃) δ 7.6(s, 1H); 7.6-6.9 (m, 4H), 6.95 (m, 2H), 4.9 (s, 2H); 3.7 (s, 3H); 2.30-2.8 (t, 2H, J=6); 2.7-2.6 (t, 2H J=6); 2.32 (s, 3H). ¹³C NMR δ 173.38, 157.16, 137.23, 135.23, 133.24, 131.96, 131.03, 130.96, 119.62, 67.80, 51.62, 30.95, 18.43.

NMR for **3.5** ¹H NMR (300MHz) (CDCl₃) δ 7.45 (s, 1H); 7.45-6.96 (m, 10H); 5.09 (s, 2H); 3.8 (s, 3H); 3.70 (s, 3H), 2.97-2.92 (t, 2H, J=6); 2.67-2.44 (t, 2H J=6); 2.20 (s, 3H). ¹³C NMR δ 173.48, 157.55, 156.51, 136.32, 135.51, 134.49, 132.84, 130.81, 130.40, 130.18, 129.95, 129.27, 129.27, 128.54, 120.83, 114.85, 111.19, 68.88, 55.52, 51.00, 36.03, 30.16, 18.70. For **3.6**: ¹H NMR (300MHz) (CDCl₃) δ 7.35 (s, 1H); 7.35-6.95 (m, 10H); 5.08 (2H); 3.8 (s, 3H); 2.97-2.91(t, 2H, J=6); 2.71-2.43 (t, 2H J=6) ; 2.4 (s, 3H). ¹³C NMR δ 178.71, 157.60, 156.49, 136.30, 135.50, 134.44, 132.48, 130.80, 130.39, 130.17, 129.26, 129.26, 128.52, 120.83, 114.95 , 111.05, 68.87, 55.51, 35.84, 29.79, 18.69.

CHAPTER III

3. ASSAYS TO EVALUATE VDR ANTAGONISTS

3.1. Luminescence and detection

Luminescence is the emission of light due to the transition of electrons from molecular orbitals of higher energy to those of lower energy, usually the ground state or the lowest unoccupied molecular orbitals. When electrons return to a ground state from being in an excited state, they release energy in the form of light (**Figure 12**).

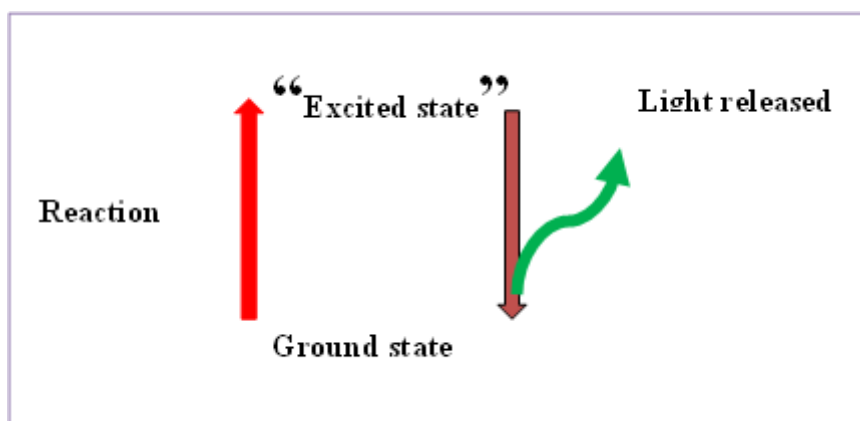


Figure 12: Schematic diagram depicting the generation of light from luminescent molecules in the excited state

Luminescence is classified according to the excited state that gives rise to it and to the source of the energy that caused the excited state to be populated with electrons. The promotion of electrons to an excited state is called excitation. In many cases, this is brought about by absorption of visible or ultraviolet radiation. In such a case, if luminescence arises because electrons are relaxing from a singlet excited state to a singlet ground state, then it is called fluorescence. If the excitation is the result of energy released in a chemical reaction, the luminescence is called chemiluminescence. A subset of chemiluminescence occurring in the biosphere as a result of biological processes is called bioluminescence.

To detect the luminescent signal, the luminometer, illustrated in Figure 13, uses the single photon counting measurement technique, which is based on a photomultiplier tube (PMT).

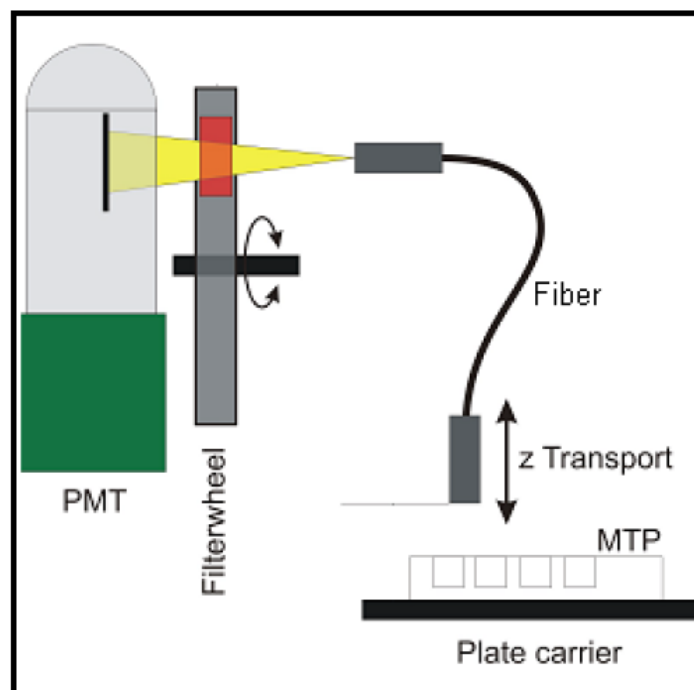


Figure 13: Luminometer detection system.

The luminescence system consists of the following parts: luminescence fiber bundle, filter wheel, and PMT detector. The luminescence fiber bundle guides the light from the sample, to the filter wheel, and finally to the detector. The filter wheel has six filter positions better isolate the analytical signal. The photon counting module (PCM) is designed to amplify and quantify the amount of light. Therefore, a photon of radiation

entering the tube strikes the cathode of the PCM, causing the emission of several electrons. These electrons are accelerated towards the first dynode. The electrons strike the first dynode, causing the emission of several electrons for each incident electron. These electrons are then accelerated towards the second dynode, to produce more electrons which are accelerated towards dynode three and so on. Eventually, the electrons are collected at the anode. Luminescence is read from the top of the well and collects as much light as possible, in order to maximize the luminescent signal. The signals from the detector are then digitalized with a computer.

3.2 Fluorescence polarization and detection

Fluorescence polarization measures the changes in the orientation of plane polarized light brought about by fluorophores that undergo rapid molecular motion during their fluorescence lifetime[29, 30]. (Figure 14)

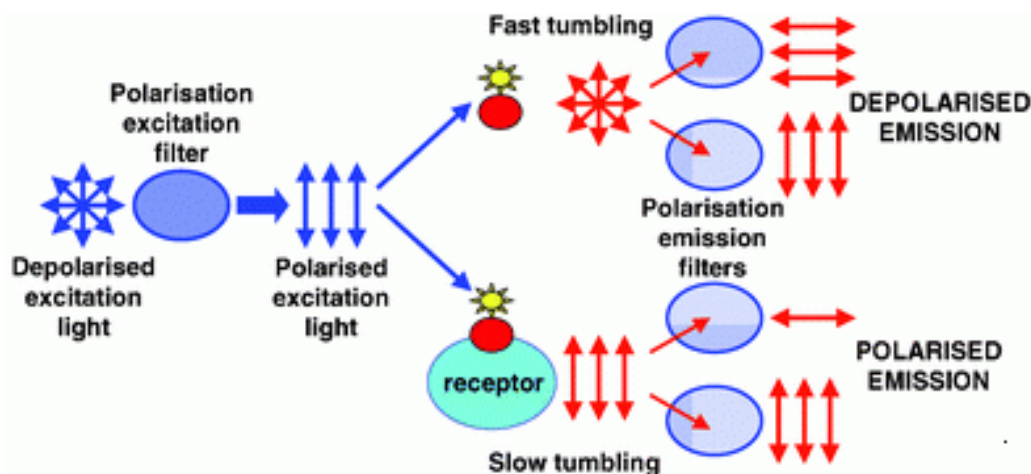


Figure 14: Fluorescence Polarization Assay principle [31]

The lifetime of fluorescence is the period of time between absorption of an excitation photon and the emission of a photon through fluorescence[30, 32]. Monochromatic light is passed through a polarization filter to generate polarized monochromatic light. The light absorbed and emitted by big fluorescent molecules remains mostly polarized and enters another parallel and perpendicular polarized emission filter detecting a high fluorescence polarization (FP) signal. In the contrary, a small fluorescent molecules depolarize light and a low FP signal is detected after a parallel and perpendicular emission filter.

For the detection of FP we were using a multi-plate reader Tecan M1000. Here, light from the light source enters the monochromator through the entrance slit (**Figure 15**).

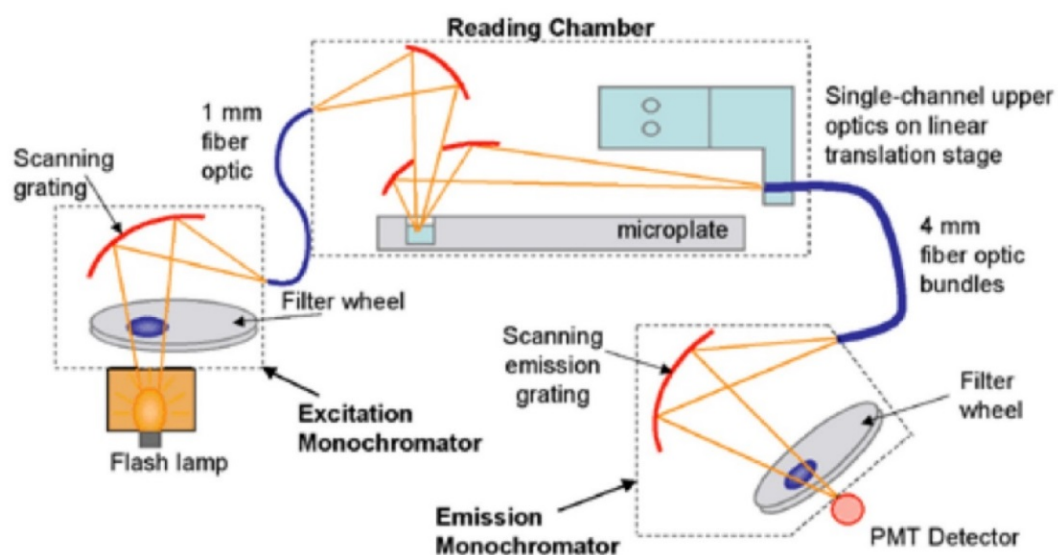


Figure 15: Fluorescence detection

The light beam is then collimated, and then strikes the dispersing element at an angle. The beam is split into its component wavelengths by the grating. Radiation of only a particular wavelength leaves the monochromator through the exit slit. The light then goes to the reading chamber and is reflected to the sample. Once the light interacts with the sample it is guided by the fiber bundle to the PMT detector.

3.3. The VDR-Coregulator FP assay

Fluorescence polarization (FP) was used to quantify the inhibition of the interaction between VDR-LBD and its coactivator protein SRC2-3 (Figure 16).[29]

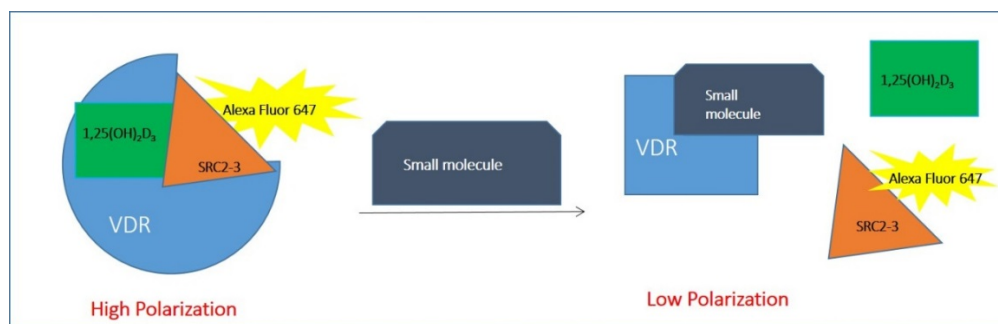


Figure 16: Cartoon of fluorescent polarization assay used to screen inhibitors

The fluorescently labeled peptide SRC2-3 molecule free in solution is excited with monochromatic polarized light at a wavelength of 635 nm. Due to its small molecular

weight, the molecule tumbles rapidly in the solution causing the emission at 685 nm of depolarized light thus a low amount of polarized light can be detected after applying a parallel and perpendicular filter. When the MBP-VDR-LBD protein binds to the ligand LG190178, the ligand-receptor complex can recruit the fluorescently labeled peptide SRC2-3. Consequently, the molecular weight of the resulting complex is increased significantly, and therefore the complex tumbles more slowly. It causes more emitted light to remain polarized in the same plane as the excitation plane. Therefore a high polarization signal is detected after applying a parallel and perpendicular filter allowing the detection of a ligand-binding to a larger macromolecule. For this assay, VDR-LBD was expressed as a MBP analog in *E. coli* and purified by affinity chromatography.[33] The coregulator peptide SRC2-3 was used because it exhibited the highest affinity towards VDR.[33] The coregulator peptide SRC2-3 was labeled with a far red AlexaFluor 647 dye to reduce the background fluorescence due to compound aggregation. In order to enable binding between VDR and SRC2-3, a synthetic analog of vitamin D referred to as LG190178[34] was used, which was identified by Ligand Pharmaceuticals[35]. The structure is shown in **(Figure-17)**.

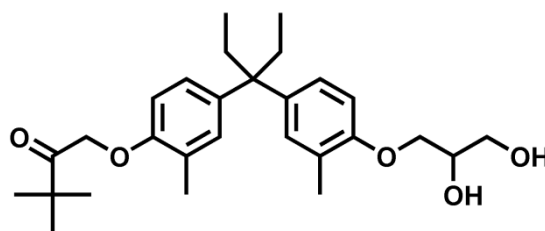


Figure 17: LG190178: Synthetic Agonist for Vitamin D Receptor.

All reagent were incubated in a volume of 0.02 ml in the presence of compound in a black 384-well plate and FP was read after 1 hour of incubation. The data was analyzed with GraphPrism.

3.4 The VDR-mediated transcription assay

The ability of VDR antagonists to inhibit VDR-mediated transcription were measured in commercially available embryonic renal cells (Hek 293T). Hek 293T cells contain, the simian vacuolating (SV) virus 40 T-antigen that allows for episomal replication of transfected plasmids containing the SV40 origin of replication. This allows for amplification of transfected plasmids and extended temporal expression of the desired gene products. This cell line is highly transfectable and grows, fairly easily, making it greatly valuable for these studies.

Two vectors, VDR-CMV, a chimeric vector bearing VDR under control of a cytomegalovirus promoter, and a second vector, 24OH luciferase, containing luciferase under control of a the 24OH promoter, were transfected into the Hek 293T cells. The luciferase reporter vector allows the quantification of VDR-mediated gene transcription, because 24OH is a VDR target gene (**Figure 18**).

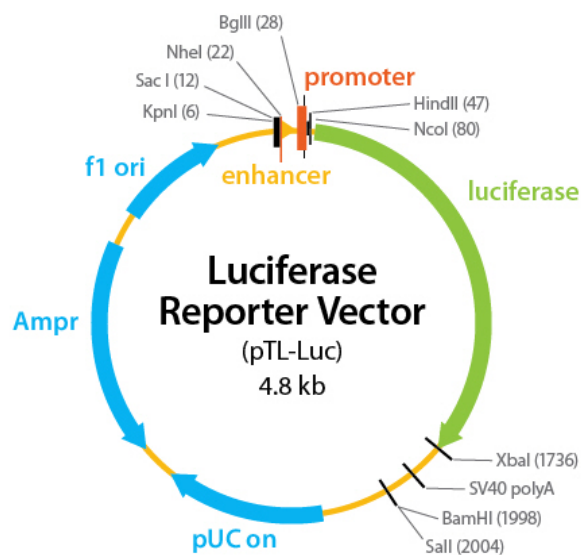


Figure 18: 24OH luciferase plasmid vector [36]

The binding between VDR and the 24OH luciferase plasmid results in the expression of luciferase enzyme that catalyzes a bioluminescent reaction. The light emitted from the chemical reaction is directly proportional to the amount of expressed enzyme, and thus, the transcriptional activity of VDR. After 18 hours, the cells are lysed and the substrate of luciferase, luciferin, is introduced into the cellular extract along with Mg and excess ATP (Figure 19).

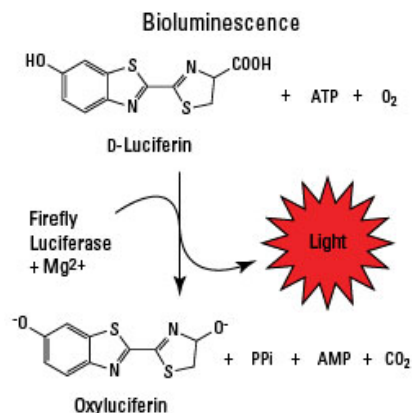


Figure 19: Enzymatic reaction of luciferase.

The luciferase enzyme acts on luciferin in the presence of magnesium cations and oxygen. The oxidation of luciferin releases energy in the form of luminescence or light.[37] The luminescence from this chemical reaction can be read and quantified by a luminescence reader. The amount of light detected from the cell lysate correlates directly with the inhibition of binding between VDR and coactivators, an interaction which is essential for VDR-mediated transcription.

3.5 Toxicity assay

The cytotoxicity of VDR antagonists was determined by luminescence using Cell Titer-Glo reagent (Promega). The cytotoxicity assay allows for the determination of the number of viable cells in culture based on quantification of the ATP present, an indicator of metabolically active cells. The toxicity assay procedure involves adding the single reagent Cell Titer-Glo Reagent directly to cell culture. The Cell Titer-Glo reagent

contains a surfactant, which causes cell lysis for ATP liberation. The APT is converted by an enzymatic reaction generating a luminescent signal that is proportional to the amount of ATP liberated. CellTiter-Glo provides the purified luciferin and luciferase necessary to measure ATP using a bioluminescent reaction.

3.6 Experimental procedures

3.6.1. Protocol to determine the interaction between VDR and coregulator SRC2-3

This assay was conducted in 384-well black polystyrene plates (Corning) using a buffer [25 mM PIPES (pH 6.75) 50 mM NaCl, 0.01% NP-40, 2% DMSO, VDR-LBD protein (0.1 μ M), LG190178 (0.75 μ M), and Alexa Fluor 647-labeled SRC2-3. Small molecule transfer into a 20 μ L assay solution was accomplished using a stainless steel pin tool (V&P Scientific), delivering 100 nL of the serially diluted compound solution (1:3 dilution starting at a 10mM concentration). Fluorescence polarization was detected after initial mixing at excitation and emission wavelengths of 650 and 665 nm (Alexa Fluor647). Three independent experiments were conducted in quadruplicate, and data were analyzed using nonlinear regression with a variable slope using GraphPadPrism software.

3.6.2. Protocol to determine the VDR-mediated inhibition of transcription

The Hek293T cells were collected from a liquid nitrogen tank and 1ml was pipetted into a 75 cm² cell culture flask containing 14ml of media, DMEM/High Glucose. The media contains non-essential amino acids, 2 mM L-glutamine, 1 mM sodium pyruvate, and 1500mg/L sodium bicarbonate. The flask is then placed in an incubator 37°C and 5 percent carbon dioxide until they reached 80 to 90 percent confluency.

Matrigel: The purpose of matrigel for this assay is to coat the bottom of the flask and the 384 well plates so that the cells can attach to the bottom. The solution is prepared by taking 100mL of phenol red-free DMEM and 250 µL of Matrigel concentrate. Matrigel is the name for a gelatinous protein secreted by mouse sarcoma. 3 ml of Matrigel solution are added to the flask and incubate for 5 minutes. The solution is replace with growth media followed by the addition of cells.

Trypsin: Trypsin-EDTA is the most commonly used method for passaging adherent cells. Trypsin treatment disrupts the cell monolayer and a proteolytically cleave the bonds between cells and cells and flask. Often gentle pipetting after trypsin treatment dissociates all cell clumps into single cells.

Lipofectamine: Allows the transfer of DNA into eukaryotic cells with minimum damage to the cells or plasmid. Since DNA is a charged molecule moving it past the hydrophobic cell membrane can be a challenge. Lipofectamine is used in lipid-based methods of transfection. The cationic head group associates with the anionic phosphates groups on the nucleic acids. A lipid-DNA complex can pass through the cell membrane, either by endocytosis or by fusion with the plasma membrane.

Plus Reagent: The Plus Reagent is used for pre-complexing DNA that enhances cationic lipid-mediated transfection of DNA into the cells.

Passaging and splitting cells: Cells could be split as early as when they are at 30% confluency. They are passaged first by aspirating the old media and then rinsing the cells with PBS buffer, which washes away dead cells floating on the flask. To detach the cells that were attached to the flask, by using 0.05 percent trypsin and incubating the flask for 5 minutes at 37°C and 5 percent carbon dioxide incubator. After 5 minutes, the cell suspension was mixed by pipette in order to achieve a single cell suspension. Cells are split into 3 new flasks. 3 ml of Matrigel is first pipetted into the new flasks and incubated at 37°C degree for 5 minutes. The matrigel is aspirated out and 14 ml of the growth media, DMEM/High Glucose (Hyclone, catalog no. SH3028401), nonessential amino acids, sodium pyruvate (1mM), HEPES (10 mM), penicillin and streptomycin, and 2%

charcoal-treated FBS (Invitrogen, catalog no. 12676-011); 1 ml of the cells in trypsin is added to each flask.

VDR Transfection: When the cells reach about 80% confluency, 2 mL of untreated DMEM containing 1.2 μL of VDR-CMV (649.7 ng/ μL) thus 0.78 μg ; 5.1 μL of 24OH-luciferase (514.2 ng/ μL) thus 15.6 μg , and 25 μL of Plus Reagent were added and incubated for 5 minutes at room temperature. After the 5 minutes, 75 μL Lipofectamine was added and the mixture was incubated for 30 minutes on the shaker at room temperature. The mixture was then added to the flask containing the cells and incubated overnight. After 18h, 3 mL of 0.05% trypsin (Hyclone, catalog no. SH3023601) was added and the mixture was incubated so that the cells were completely detached from the bottom of the flask. After converting the mixture into a single cell solution by pipetting up and down a few times. The trypsinized cells were added to 12 mL of DMEM/High Glucose (Hyclone, catalog no. SH3028401), nonessential amino acids, sodium pyruvate (1 mM), HEPES (10 mM), penicillin and streptomycin, and 2% charcoal-treated FBS (Invitrogen, catalog no. 12676-011), and spun down for 2 min at 1000 rpm. The media is removed leaving behind the pellets at the bottom. The cells were re-suspended in the same medium and diluted to 16 mL. 20 μL of Matrigel was added into rows of white clear bottom 384-well plates and incubated at 37°C for 5 minutes. The Matrigel solution is removed from 384 well plate and 20 μL of the cell solution was added to specific rows on the plate. The plates are centrifuged and incubated for five hours. After the 5 hours,

compounds and control plates were added to cells using the Pintool (2x transfer of compounds and 1x transfer of control plate) and incubated for 18 hours. Controls are, DMSO (negative) and cell with were not treated with agonist calcitriol. After the 18 hours, the Bright Glo luciferase reagent was warmed up and 20 ul of it was added to each well containing the cells. After a quick shake on a shaker and centrifugation at 1000 rpm for one minute the plate was incubated for 20 minutes. Luminescence was measured using Tecan M1000 and % inhibition was determined using the controls.

3.6.3. Protocol to determine the PPAR δ -mediated inhibition of transcription

The assay for the PPAR δ was performed the same way as the VDR-mediated transcription assay except, 1500ng of PPAR δ GAL4 (814.4 ng/ μ L) and 16,000ng GAL4REluc (543.1 ng/ μ L) were added. The same amount of Plus Reagent and Lipofectamine were used. On the control plate, GW7647 (30 nM), a PPAR δ agonist, was used as a positive control and DMSO was used as a negative control.[38]

Preparation of drug plates: The compound plate was prepared by first dissolving the compound in DMSO to get 10mM solution. 90 μ L of 10 mM solution of the small molecule was put in the first well of a 96-well plate and a 1:3 dilution was made in DMSO filling rows 1 to 10. Using the multi-channel pipette, 20 μ L of serial diluted small

molecule were pipetted to 384 well opaque drug plate filling rows 1 to 20. The experiment was done in quadruplets A1, A2, B1, B2; all have the same concentration. A second 384-well polystyrene plate, the control plate, had calcitriol on wells 1-20 and positive and negative controls. DMSO was the negative control for the antagonist assay. For the agonist assay, the control plate had DMSO as a positive control and calcitriol as a negative control.

3.6.4 Protocol to determine the viability of cells

Hek 293T cells were also used for this assay and were cultured, plated, and drugged in the same manner as described in the transcription assay chapter. Cells were plated the same way in a 384 well plate. After 5 hours the compound and control were added to the cells and incubated at 37 °C for 18 hours. To perform the luciferase assay, 20 µL of the Cell Titer-Glo reagent was added to each well of the 384-well plate that contained the cells using a multi-channel pipette. The plate was centrifuged for 2 minutes at 1,000 rpm and allowed to sit for 20 minutes. The Tecan Infinite M-1000 multi-label reader was used to measure the amount of luminescence generated from each well.

CHAPTER IV

4. SUMMARY OF RESULTS

4.1 BF050813G

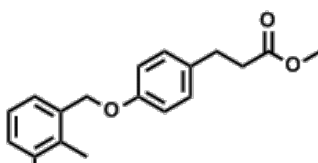
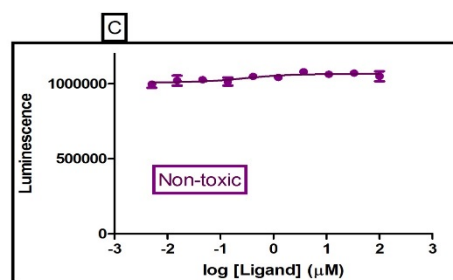
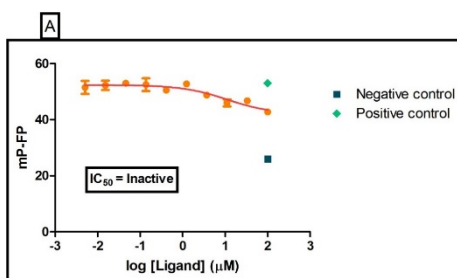


Figure 20: Summary of BF050813G; A) FP; B) VDR-mediated transcription (antagonist mode); C) Toxicity; D) PPAR δ -mediated transcription (agonist mode)

The FP assay, BF050813G did not show a significant change in signal and hence no IC₅₀ values were calculated (**Figure 20A**). However, VDR-mediated transcription was inhibited (significant decrease in the luminescence) at higher concentrations with an IC₅₀ value of 43 μ M (**Figure 20B**). In addition, there was also no signal change for the PPAR δ activity (**Figure 20D**), and toxicity assays (**Figure 20C**).

4.2 BF040813F

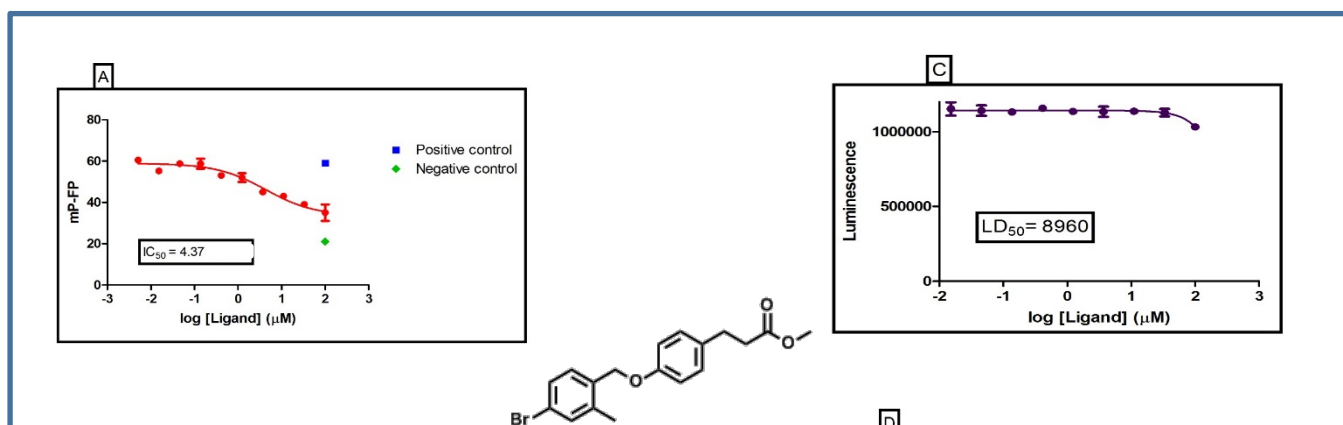


Figure 21: Summary of BF040813F; A) FP; B) VDR-mediated transcription (antagonist mode); C) toxicity; D) PPAR δ -mediated transcription (agonist mode)

Compound BF040813F showed activity towards VDR in both, the fluorescence polarization assay (**Figure 21A**) and VDR-mediated transcription assay (**Figure 21B**), with $IC_{50} \sim 4.37 \mu M$ and $IC_{50} = 13.96 \pm 3.54 \mu M$, respectively. BF040813F is not toxic and is not active as PPAR δ agonist (**Figure 21C & D**).

4.3 BF060813H

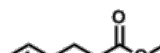
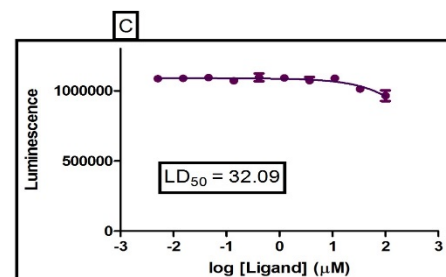
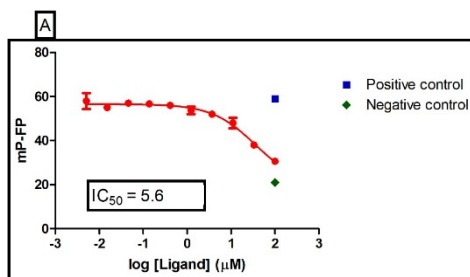


Figure 22: Summary of BF060813H; A) FP; B) VDR-mediated transcription (antagonist mode); C) toxicity; D) PPAR δ -mediated transcription (agonist mode)

BF060813H is active in fluorescence polarization assay with an IC₅₀ of ~5.6 μ M (**Figure 22A**). The activity in cells for the VDR-mediated transcription assay is IC₅₀ = 32.57 \pm 7.55 μ M (**Figure 22B**). BF060813H is nontoxic and is not able to activate PPAR δ -mediate transcription (**Figure 22C&D**).

4.4 BF090713B

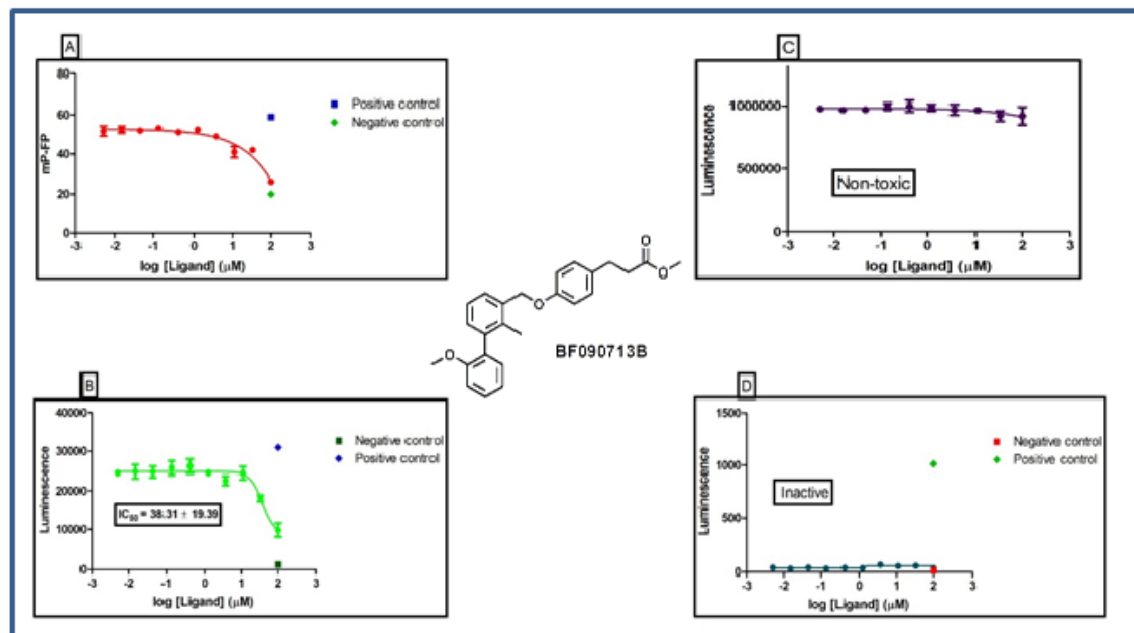


Figure 23: Summary of BF090713B; A) FP; B) VDR-mediated transcription (antagonist mode); C) toxicity; D) PPAR δ -mediated transcription (agonist mode)

Although activity is observed for BF090713B in the VDR FP assay a non-linear regression was not possible due to missing data points at higher concentrations (**Figure 23A**). The IC₅₀ value for the VDR-mediated transcription study was 38.31 ± 19.39 μM (**Figure 23B**). BF090713B is nontoxic (**Figure 23C**) and has no agonistic activity with PPAR δ (**Figure 23D**).

4.5 BF090613C

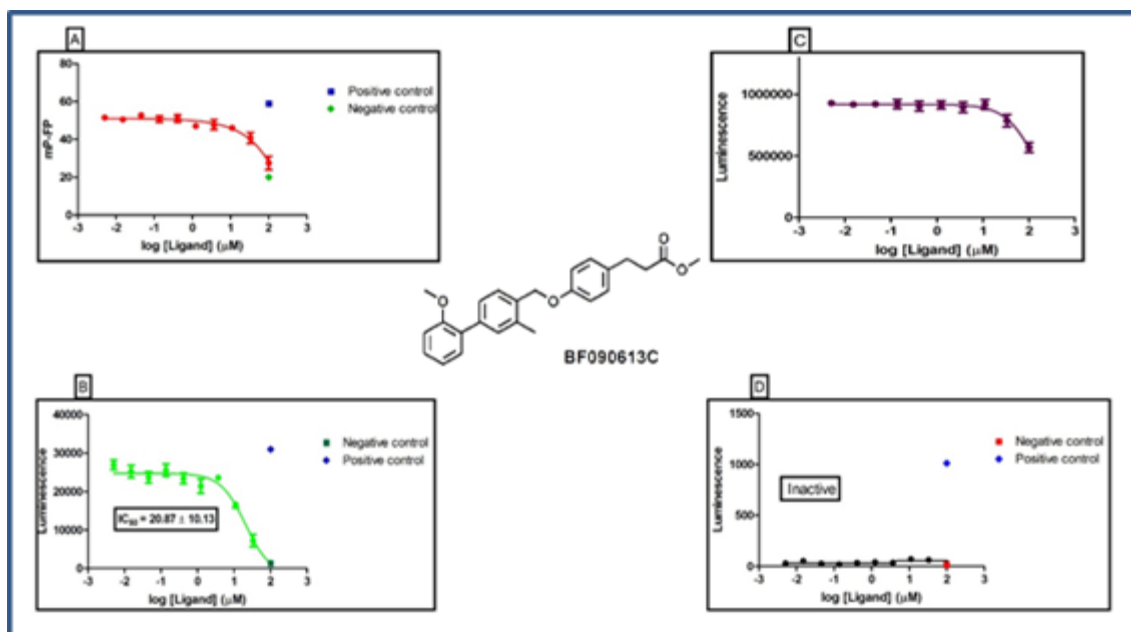


Figure 24: Summary of BF090613C; A) FP; B) VDR-mediated transcription (antagonist mode); C) toxicity; D) PPAR δ -mediated transcription (agonist mode)

The IC₅₀ values could be calculated accurately for compounds BF090613C in the transcription assay, which was $20.87 \pm 10.13 \mu\text{M}$ (**Figure 24B**). However, as mentioned above, the accurate calculation of the IC₅₀ values was not possible for the fluorescence polarization assay due to insufficient data (**Figure 24A**). Compound BF090613C also showed toxicity between $30 \mu\text{M}$ and $100 \mu\text{M}$ (**Figure 24C**). Compared to the previously described compounds, this compound has shown the highest toxicity. There was no transcriptional activation of the PPAR δ (**Figure 24D**).

4.6 BF090813A

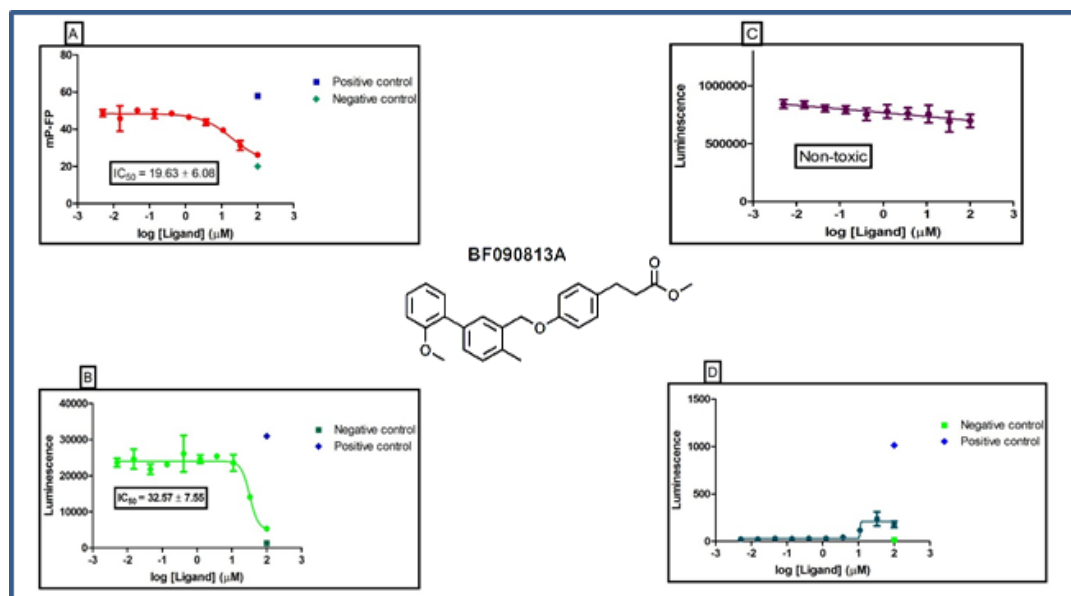


Figure 25: Summary of BF090613C; A) FP; B) VDR-mediated transcription (antagonist mode); C) toxicity; D) PPAR δ -mediated transcription (agonist mode)

Compound BF090813A is a VDR antagonist indicated by both the fluorescence polarization (**Figure 25A**) and VDR-mediated transcription assay (**Figure 25B**) with an IC_{50} values of $19.63 \pm 6.08 \mu\text{M}$ and $32.57 \pm 7.55 \mu\text{M}$ respectively. BF090813A did not show toxicity at the concentrations tested (**Figure 25C**) but showed a partial agonist behavior with PPAR δ . 8% activity was observed at concentration of $100 \mu\text{M}$ BF090813A (**Figure 25A**).

4.7 BF090712D

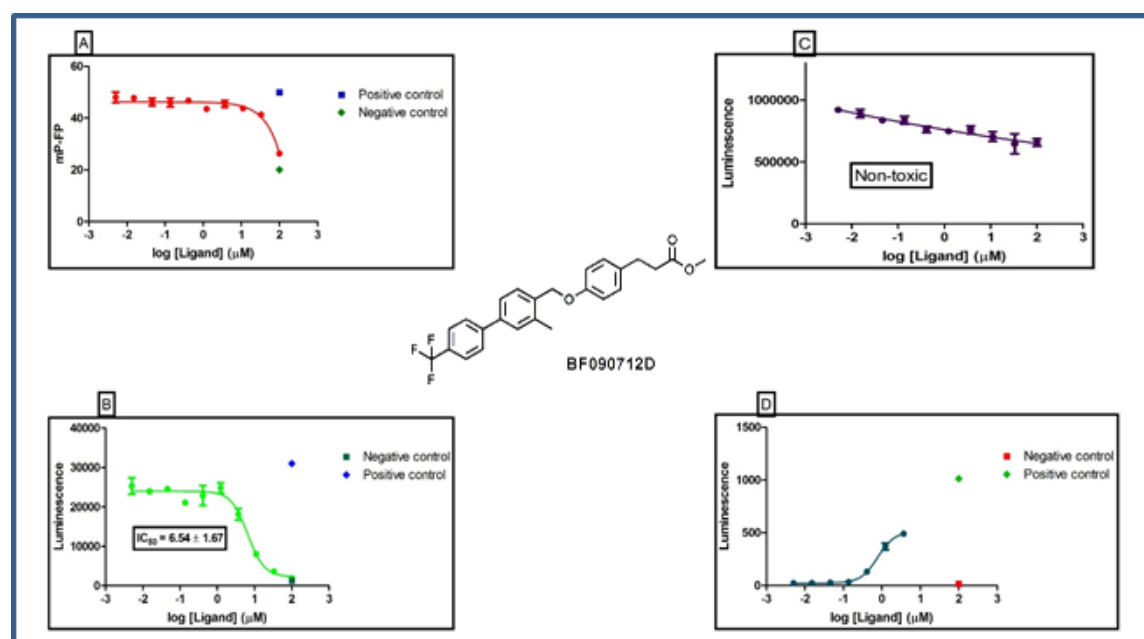


Figure 26: Summary of BF090712D; A) FP; B) VDR-mediated transcription (antagonist mode); C) toxicity; D) PPAR δ -mediated transcription (agonist mode)

Compound BF090712D shows activity at higher concentrations in the fluorescence polarization assay but an IC_{50} value calculation was not possible due to insufficient data (**Figure 26A**). The transcription assay (**Figure 26B**), however, shows

the compound is an antagonist with an IC_{50} value of $6.54 \pm 1.7 \mu\text{M}$. This compound is also nontoxic as most of the other analogues (**Figure 26C**). BF090712D is able to activate transcription mediated by $\text{PPAR}\delta$. There is 32% activity at $0.5 \mu\text{M}$ in comparison with $\text{PPAR}\delta$ agonist GW7647 (**Figure 26D**).

4.8 BF090713B1

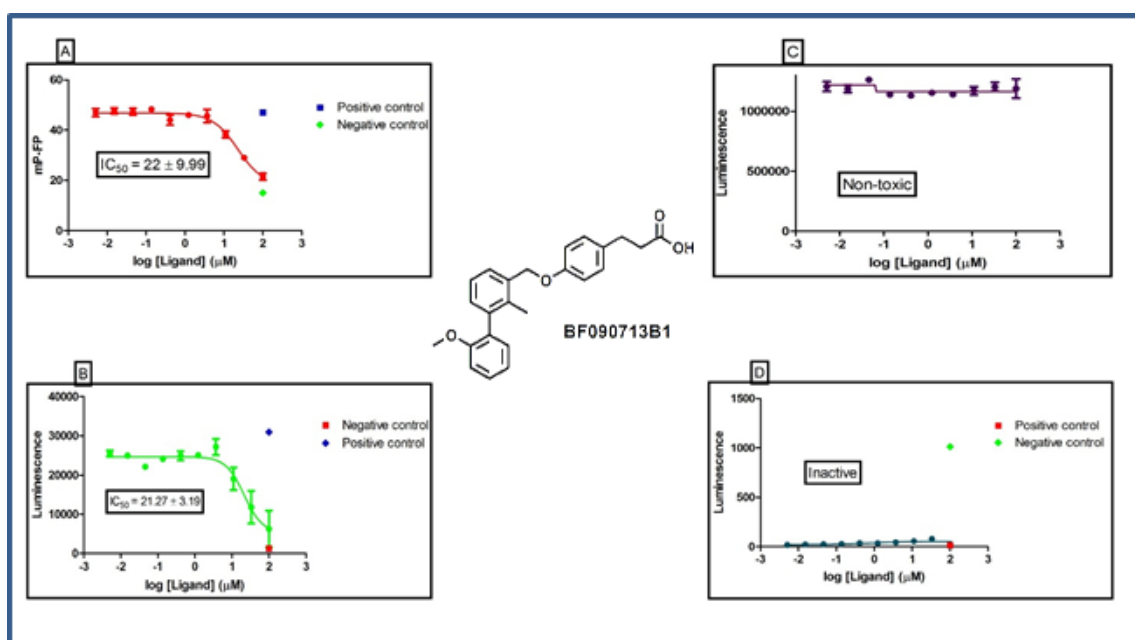


Figure 27: Summary of BF090613B1; A) FP; B) VDR-mediated transcription (antagonist mode); C) toxicity; D) PPAR δ -mediated transcription (agonist mode)

Compound BF090713B1 is a VDR antagonist as determined by the FP and transcription assays. IC_{50} values determined for both assays are very similar, $22.0 \pm 9.99 \mu\text{M}$ and $21.27 \pm 3.19 \mu\text{M}$ for the FP (**Figure 27A**) and transcription assays (**Figure 27B**), respectively. This compound was also determined to be nontoxic at the concentrations tested (**Figure 27C**). There was also no activity with $PPAR\delta$ (**Figure 27D**).

4.9 BF090613C1

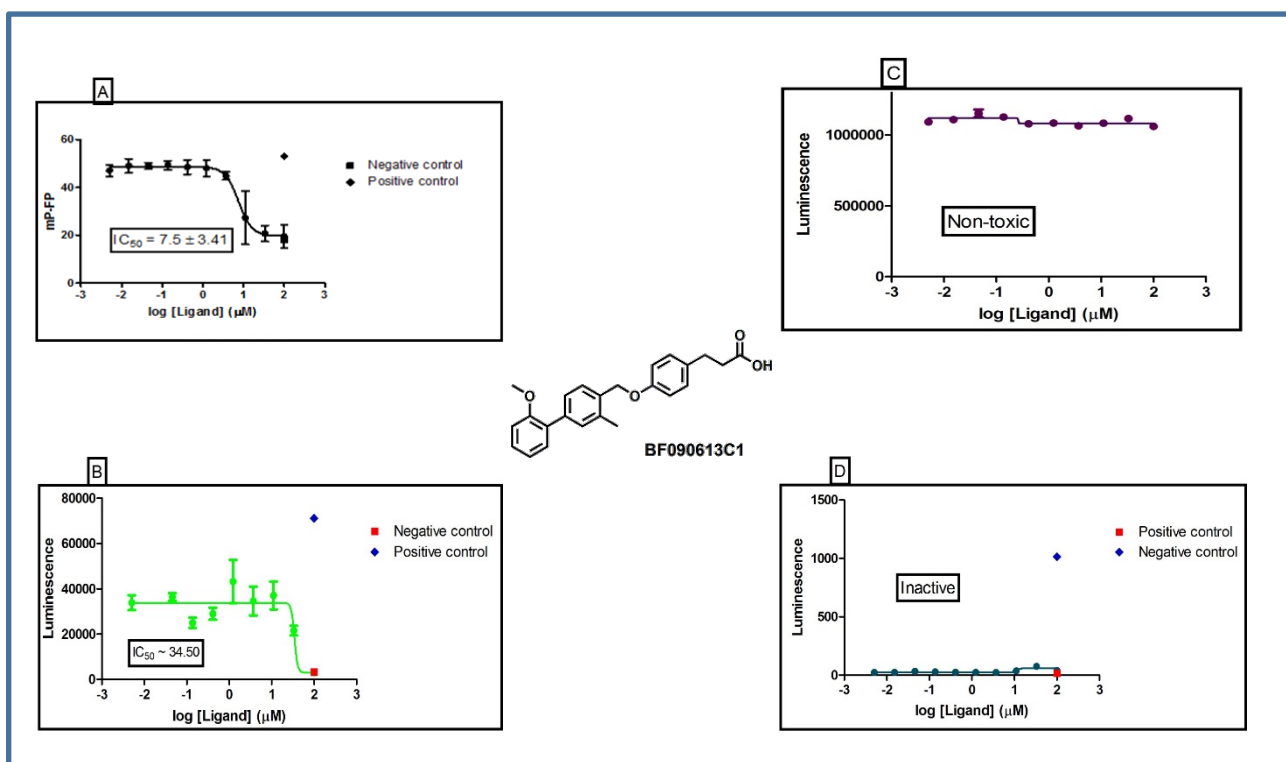


Figure 28: Summary of BF090613C1; A) FP; B) VDR-mediated transcription (antagonist mode); C) toxicity; D) $PPAR\delta$ -mediated transcription (agonist mode)

Compound BF090613C1 is active in the VDR FP assay and the VDR mediated transcription assay. The IC_{50} value in the FP assay (**Figure 28A**) is $7.5 \pm 3.41 \mu\text{M}$ and the IC values of the transcription assay (**Figure 28B**) is $34.50 \mu\text{M}$. BF090613C is not toxic (**Figure 28C**) and is not able to activate PPAR δ -mediated transcription (**Figure 28D**).

4.10 BF090813A1

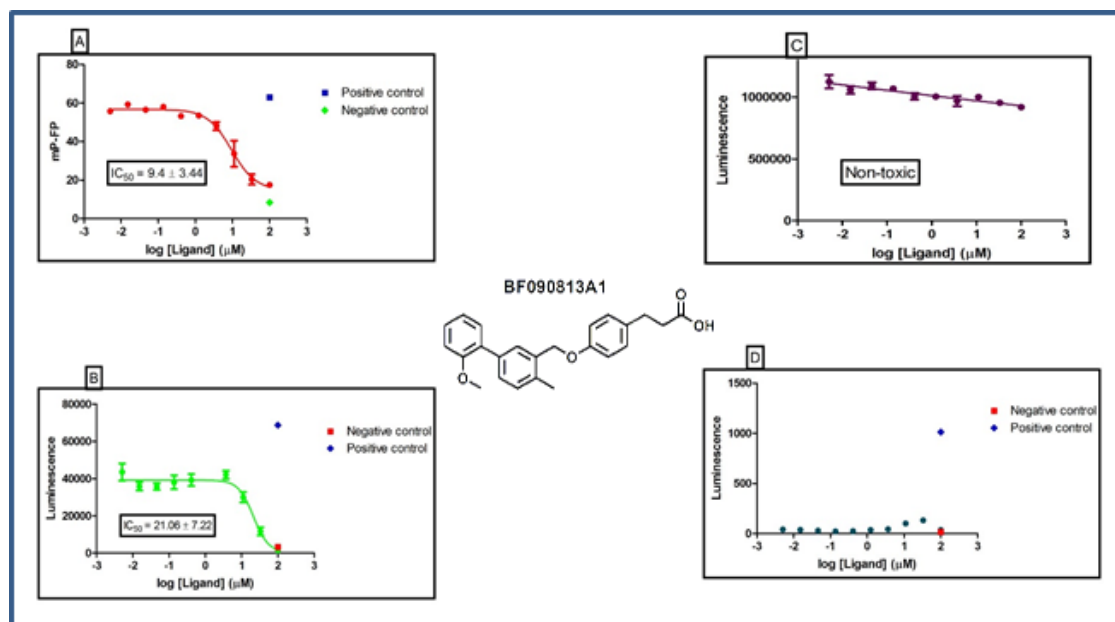


Figure 29: Summary of BF090613C1; A) FP; B) VDR-mediated transcription (antagonist mode); C) toxicity; D) PPAR δ -mediated transcription (agonist mode)

Compound BF090813A1 is active in the FP assay ($IC_{50} = 9.4 \pm 3.44 \mu M$) (**Figure 29A**) and in the transcription assay (**Figure 29B**) ($IC_{50} = 21.06 \pm 7.2 \mu M$). This VDR antagonist is nontoxic (**Figure 29C**). In terms of agonistic activity with PPAR δ , there is 8% activity at 40 μM (**Figure 29D**).

4.11 F090812E

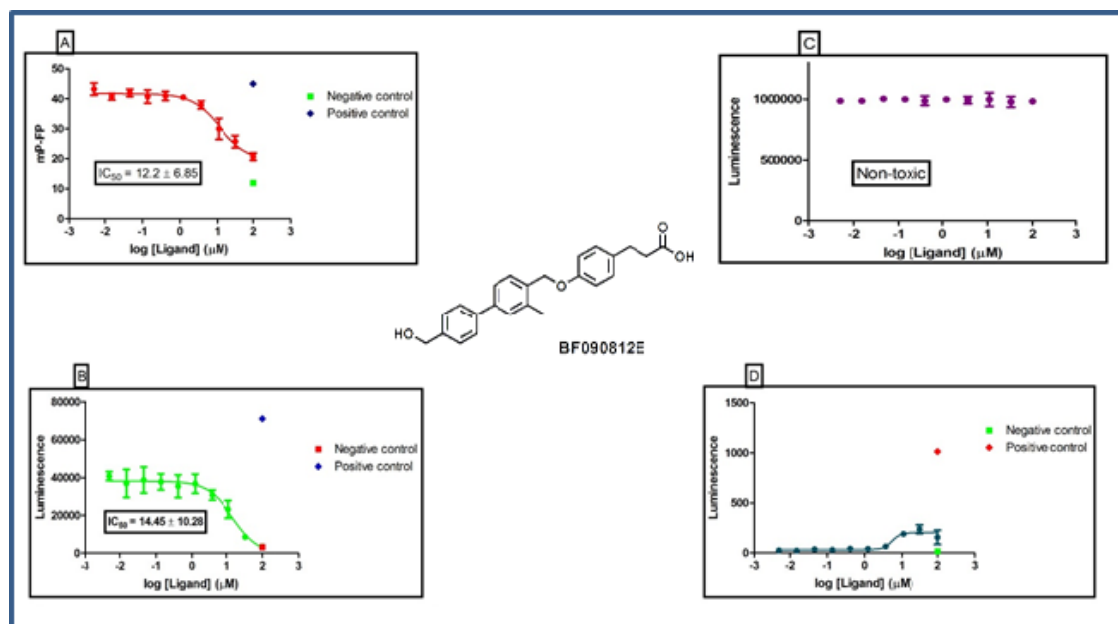


Figure 30: Summary of BF090613C1; A) FP; B) VDR-mediated transcription (antagonist mode); C) toxicity; D) PPAR δ -mediated transcription (agonist mode)

Compound BF090812E is also an antagonist of VDR as determined by the FP and Transcription assays. IC₅₀ values determined for both assays are very similar, 12.2 ± 6.8 μ M (**Figure 30A**) and 14.4 ± 10.2 μ M (**Figure 30B**) for the FP and transcription assays, respectively. This compound was also determined to be nontoxic at the concentrations tested (**Figure 30C**). In addition, minor PPAR δ activity (**Figure 30D**) was detected with an activation of 19% in comparison with agonist GW7647 at concentration of 10 μ M.

CHAPTER V

5. DISCUSSION AND CONCLUSIONS

In total, 11 compounds were investigated with respect to their ability to bind VDR and inhibit the recruitment of coagulators. The design of the compounds was based on the scaffold of GW0742, a potent PPAR δ agonist, substituting the thiazole moiety with a phenyl ring. The compounds also exhibit a different connectivity of the two moieties of the GW0742 scaffold, which was realized with the thiazole-phenyl switch. The goal of this research was, in respect to GW0742, to improve the affinity towards VDR and reduce the agonistic effects towards PPAR δ .

The activity of compounds was measured with a biochemical FP assay that determines the inhibition of VDR binding to coregulator peptide SRC2-3. All of the scaffolds demonstrated the ability to inhibit the VDR-SRC2-3 interaction. The compounds were also tested towards their ability to bind unliganded VDR and enable the recruitment of SRC2-3 in an agonist mode. None of the compound were VDR agonists (results not shown). On the other hand, they all show some level of inhibition in the antagonist mode. The most active inhibitor was compound BF060813H, a precursor for

the final compound BF090813A1, which is an active VDR antagonist as well. The other precursors BF050813G and BF060813H had a much lower activity. The final carboxylic acid compounds BF090813A1, BF090713b1, and BF090613C1 bearing a methoxy substituent were significantly more active than the corresponding methyl ester compounds BF090713B, BF090613C, and BF090813A.

In addition, all compound were investigated using a VDR-mediate transcription assay. In cells, the inhibition of VDR-coactivator interactions will result in the inhibition of transcription; in this case the transcription of the luciferase enzyme. Among the precursor compounds BF060813H, which also exhibited high activity in the FP assay was able to inhibit VDR-mediated transcription in cells with an IC_{50} value of 4.3 μ M. The other precursors BF050813G and BF060813H were less active. The methyl ester compounds BF090713B, BF090613C, and BF090813A, similar to the results of the FP assay, were less active than the final carboxylic acid compounds. The methyl ester BF090712D, however, exhibited a high activity in the cell-based assay but weak activity in the FP assay. In addition, we observed a decreasing cell viability at higher concentration of BF090712D, which in addition to inhibition of transcription will lower the luminescence signal due to the decreased amount of viable cells. All final products BF090813A1, BF090713b1, BF090613C1, and BF090812E showed a good activity in the transcription assay without any signs of toxicity. Compound BF090812E was the most active among these final compound with an IC_{50} of 14.4 μ M.

Because these compounds were structurally derived from GW0742, a PPAR δ agonist, the activity of all compounds towards PPAR δ was determined. Only three compounds showed a partial activity towards PPAR δ , which include BF090813A, BF090712D, and BF090812E. The methyl ester BF090712D was the most potent PPAR δ agonist with an IC₅₀ value of around 1 μ M and an activation of almost 50% in respect to GW7647. The methyl ester BF090813A was significantly less active than BF090712D with an 8% activity in respect to GW7647 at 100 μ M. Finally, BF090812E, bearing a hydroxymethyl group instead of a methoxy group is the only final compound that activated PPAR δ transcription at a level of 19% at 100 μ M.

Overall a series of new VDR antagonists were generated and evaluated using several biochemical and cell-based assays. The introduction of a 2-methoxy group minimized the activity of the final compounds towards PPAR δ , which was confirmed by the elevated PPAR δ activity of 4-hydroxy substituted compounds BF0908122E. The methyl ester compounds were generally less active in the FP assay than in the cell-based assay, which might have to do with the poor solubility but good permeability of these compounds. BF090813A1 was the most active compounds towards VDR without residual activity towards PPAR δ . Surprisingly, among the precursor compounds, BF040813F exhibited a similar VDR activity and selectivity than BF090813A1. The synthesis of BF040813F, in comparison with BF09081A1, is shorter and the molecule can be produced in a higher yield. A possible continuation of this program might use

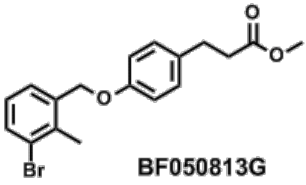
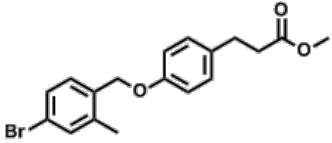
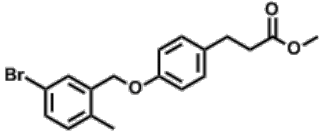
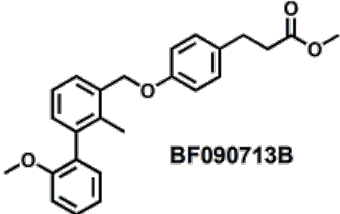
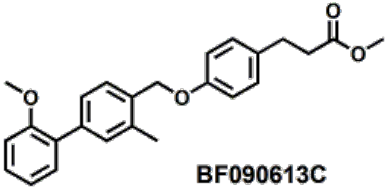
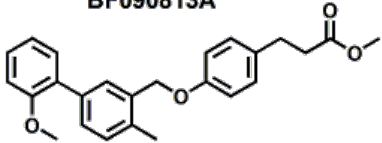
BF040813F as parent compound and investigate the ability of compounds similar to BF040813F to inhibit VDR-mediated transcription.


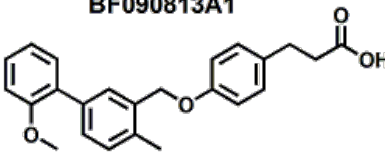
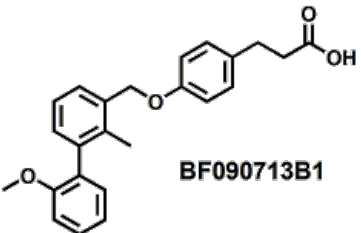
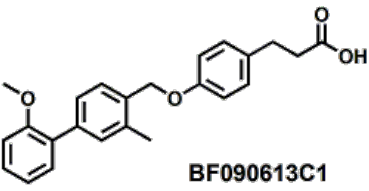
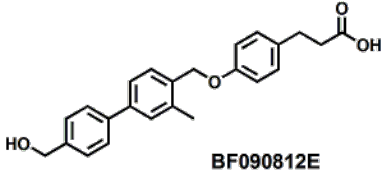
CHAPTER VI

1. SUMMARY OF DATA

Table 1: Summary of the compounds tested, with respect to their ability to inhibit VDR-mediated transcription, VDR-SRC2-3 interaction (FP assay), as well as their cytotoxicity. All results are given in micromolar concentrations.

Structure and ID	VDR-SRC2-3 interaction IC ₅₀ Values (μ M)	Inhibition of VDR-Mediated Transcription IC ₅₀ Values (μ M)	Transcription Assay: PPAR α Agonist (EC ₅₀) μ M	Toxicity (LD ₅₀) μ M
------------------	--	---	---	---

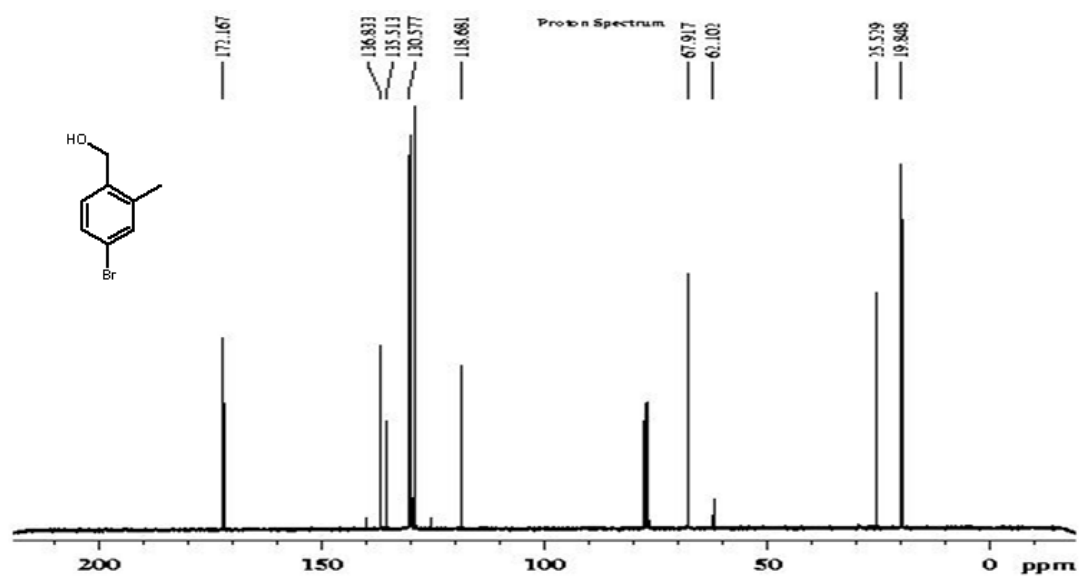
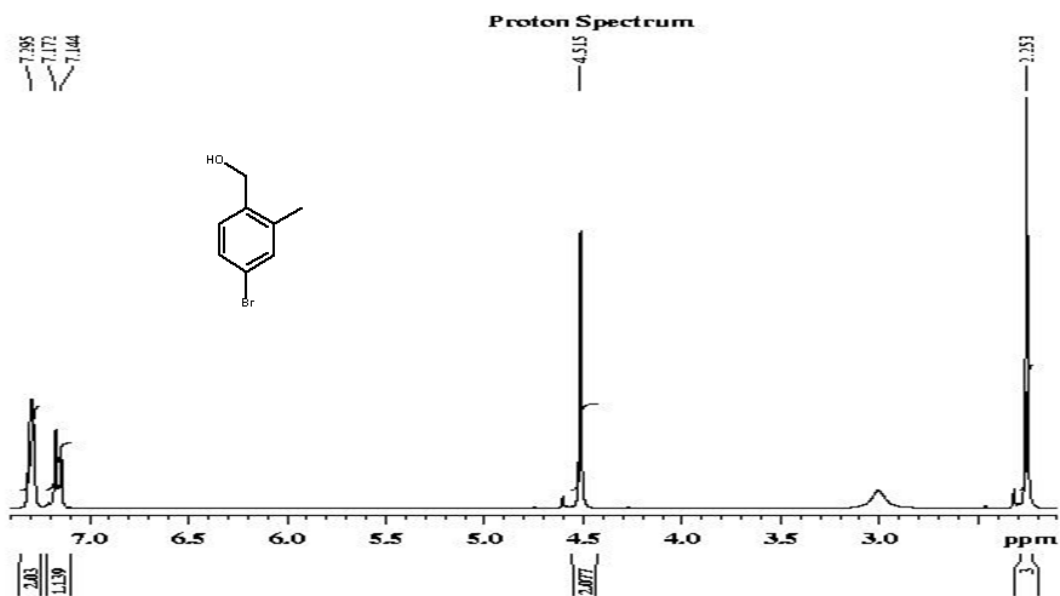
 <p>BF050813G</p>	Low activity	43.19	No Activity	Non-Toxic
 <p>BF040813F</p>	4.37	13.96	No Activity	Non-Toxic
 <p>BF060813H</p>	5.6	32.57	No Activity	Non-Toxic
 <p>BF090713B</p>	Low activity	38.31	No Activity	Non-Toxic
 <p>BF090613C</p>	Low activity	20.87	No Activity	Toxic at 100 uM
 <p>BF090813A</p>	19.63	32.57	8% activity	Non-Toxic

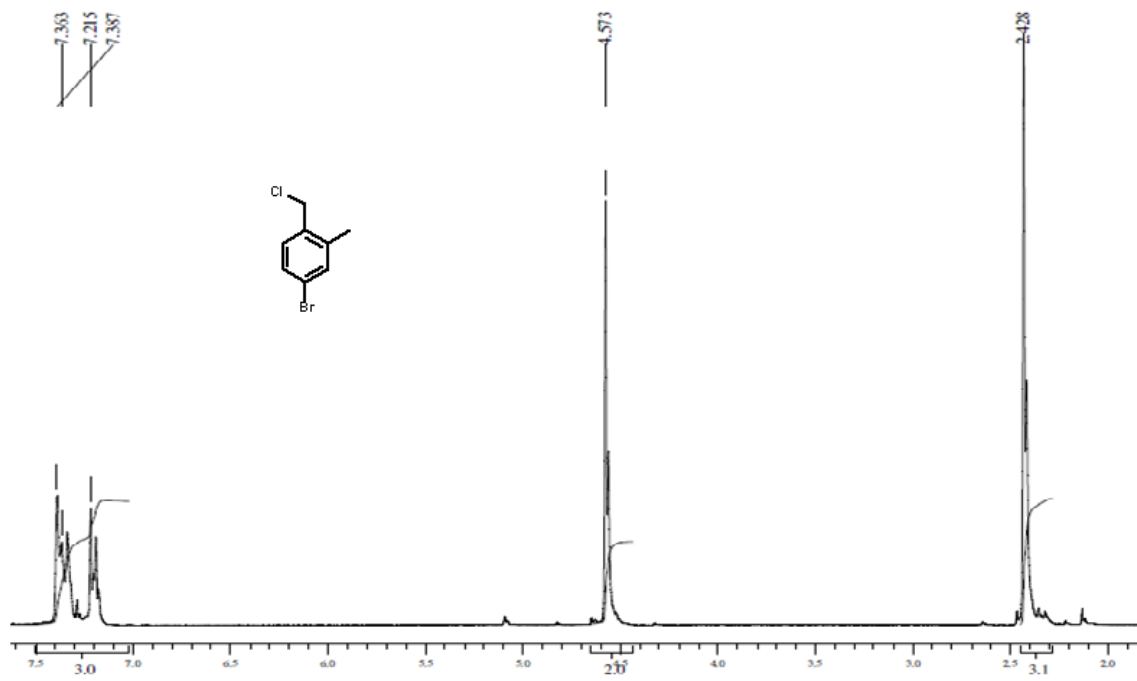
 <p>BF090712D</p>	Low activity	6.54	32 % activity	Non-Toxic
 <p>BF090813A1</p>	9.40	21.06	No Activity	Non-Toxic
 <p>BF090713B1</p>	22.00	21.27	No Activity	Non-Toxic
 <p>BF090613C1</p>	7.5	34.5	No Activity	Non-Toxic
 <p>BF090812E</p>	12.20	14.45	19%	Non-Toxic

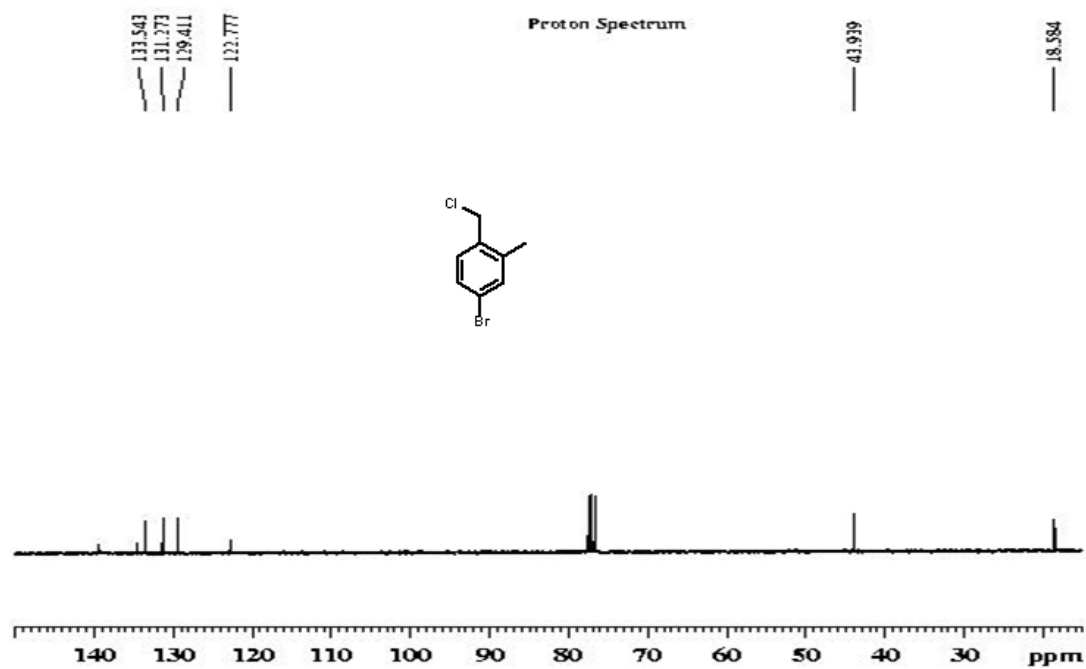
CHAPTER VII

^1H -NMR AND ^{13}C -NMR

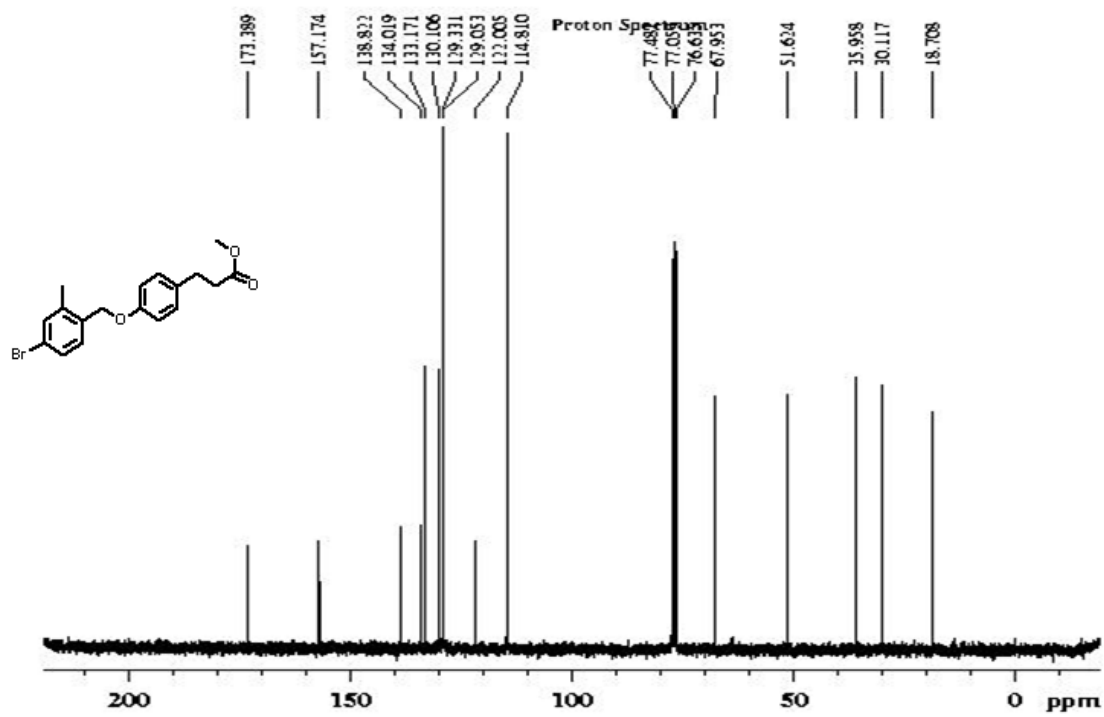
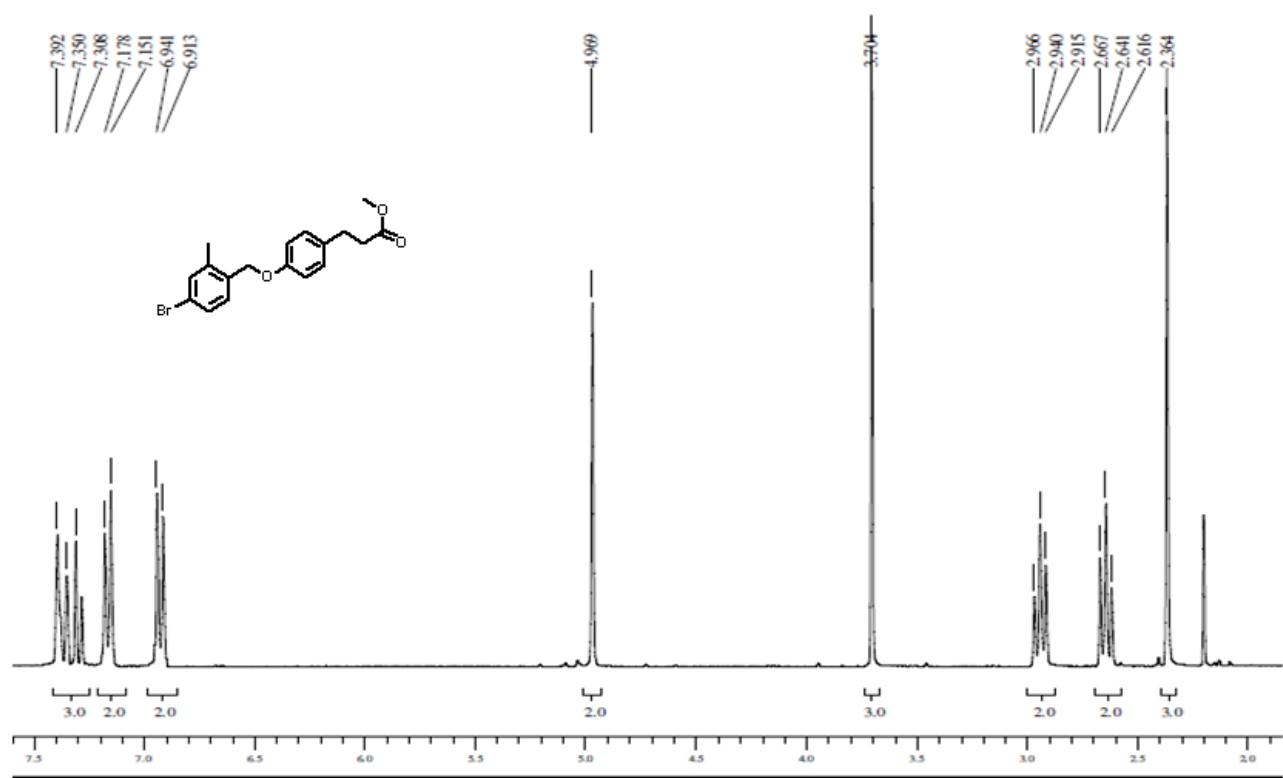
Compound 1.2



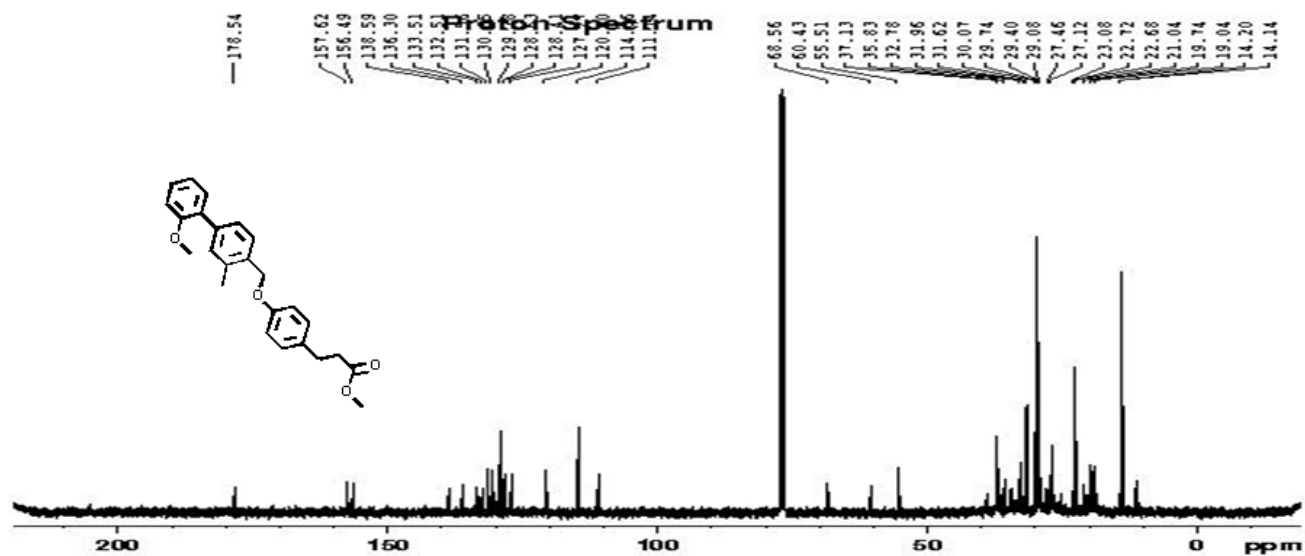
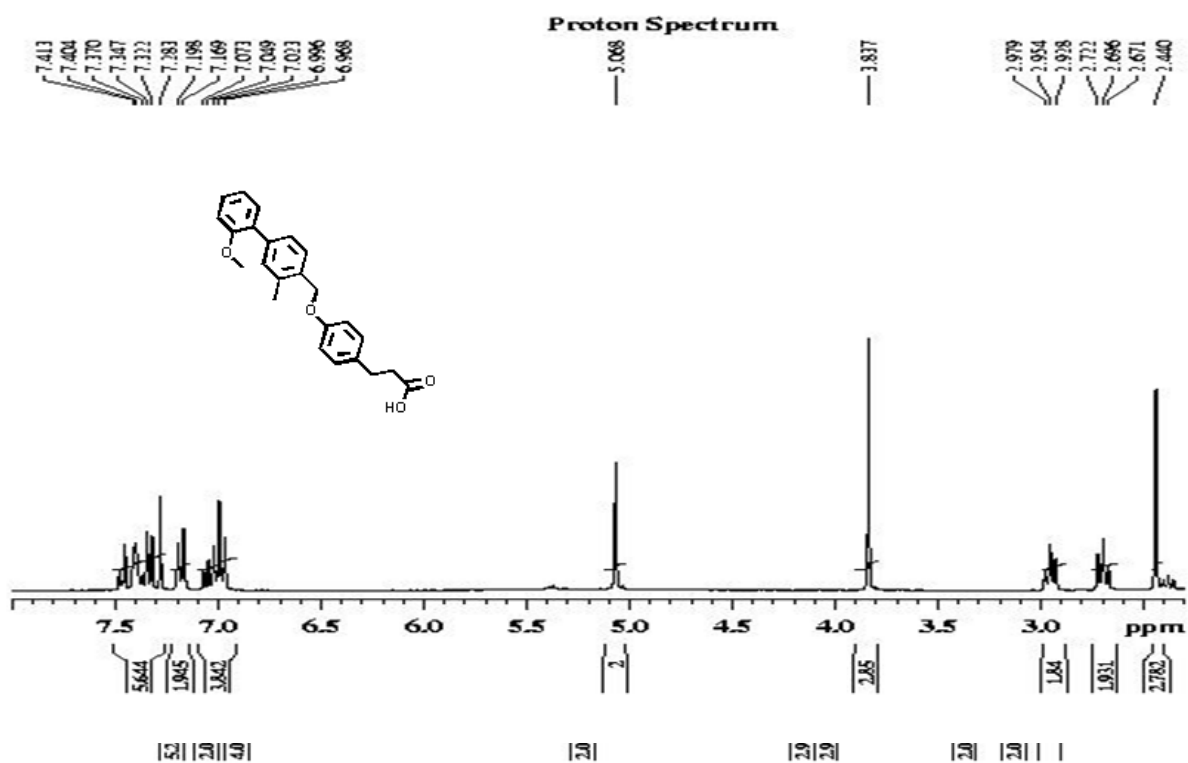
Compound 1.3



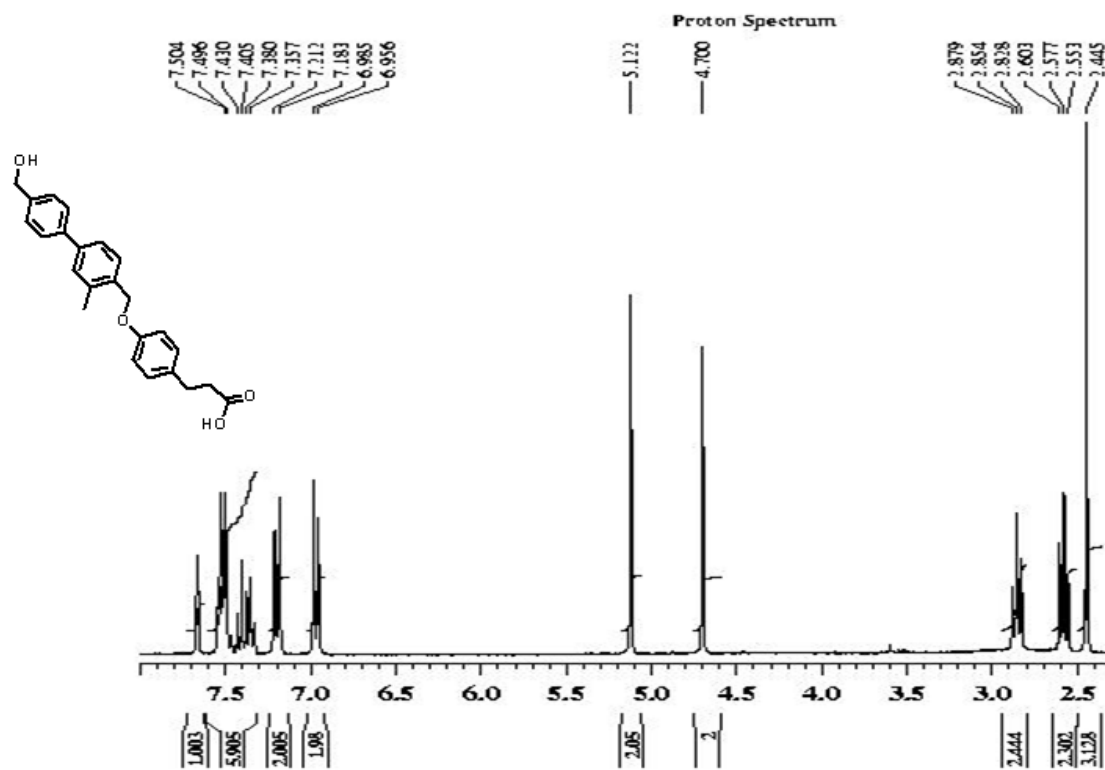
Compound BF040813F

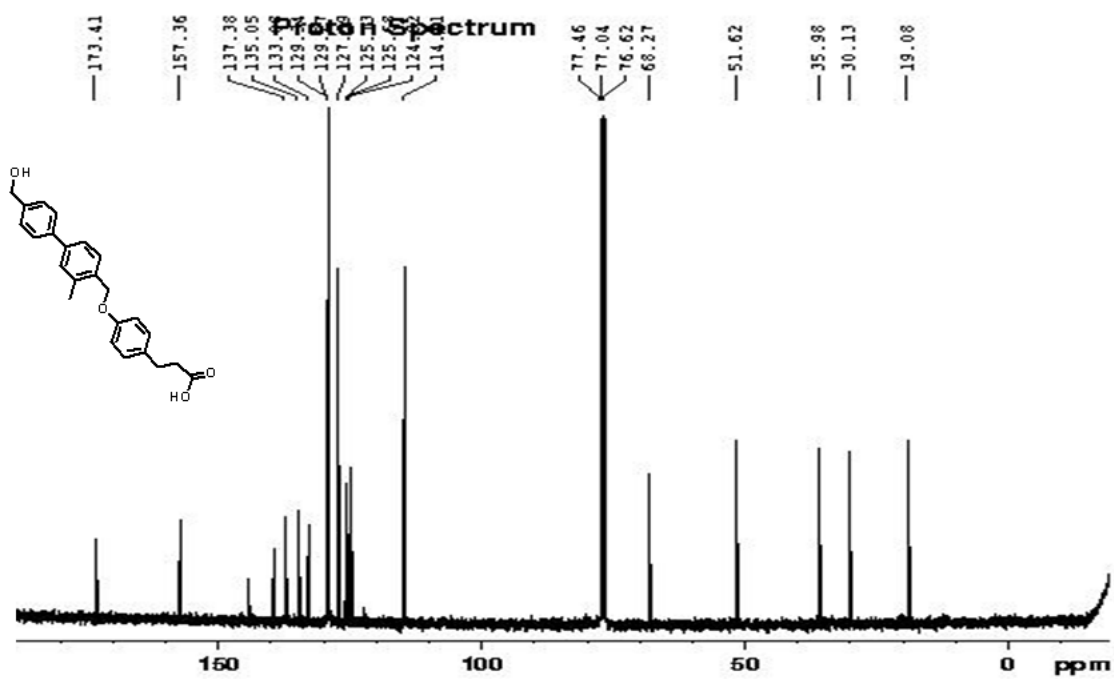
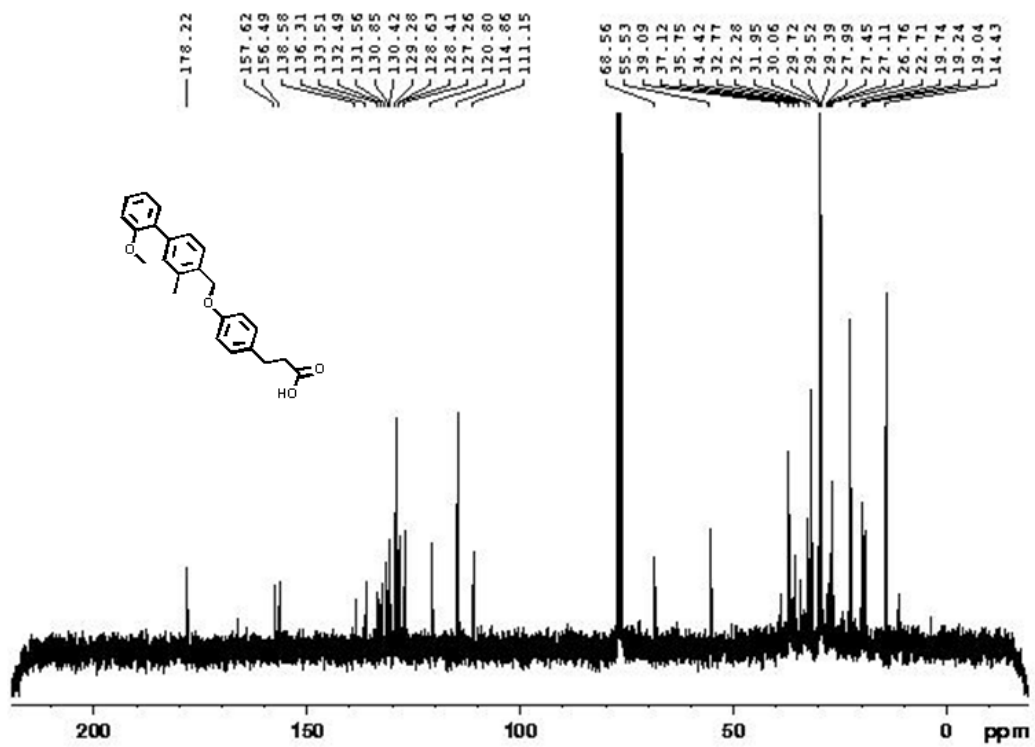


Compound BF090613C

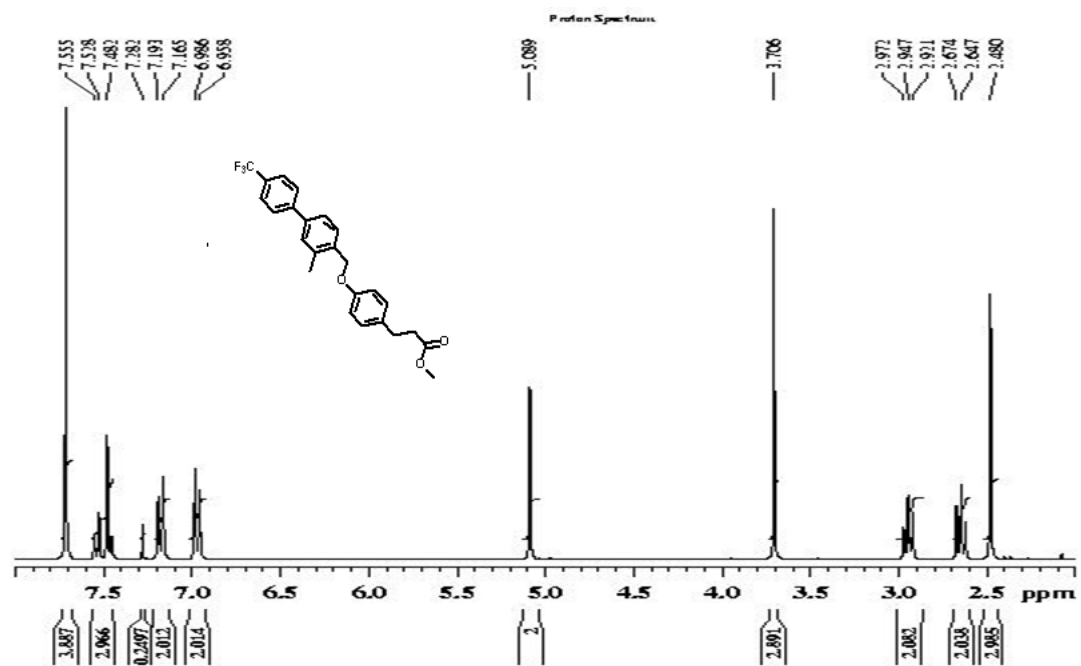


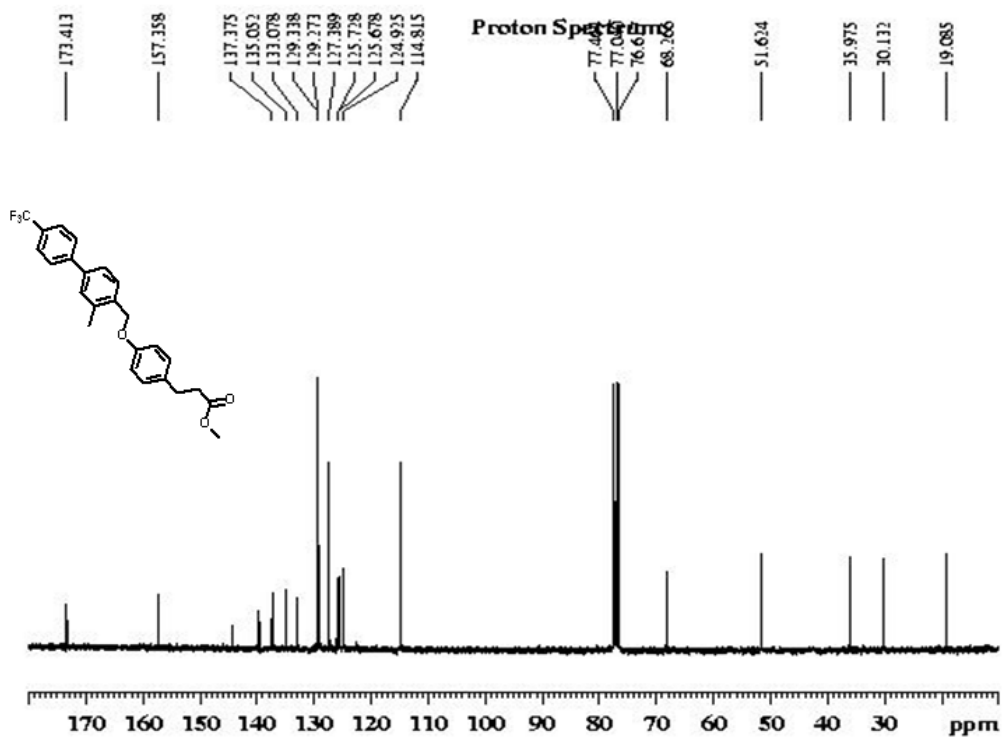
Compound BF090812E



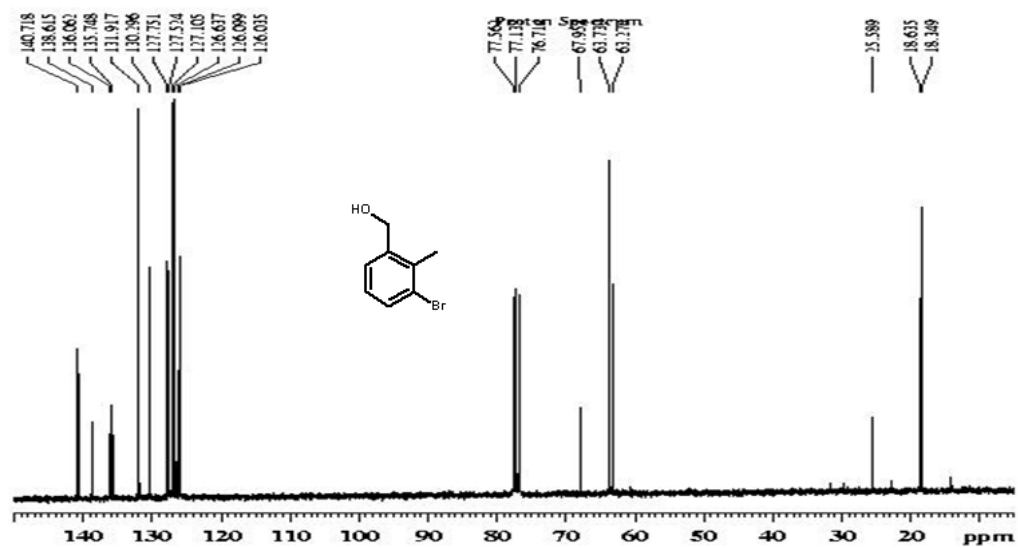
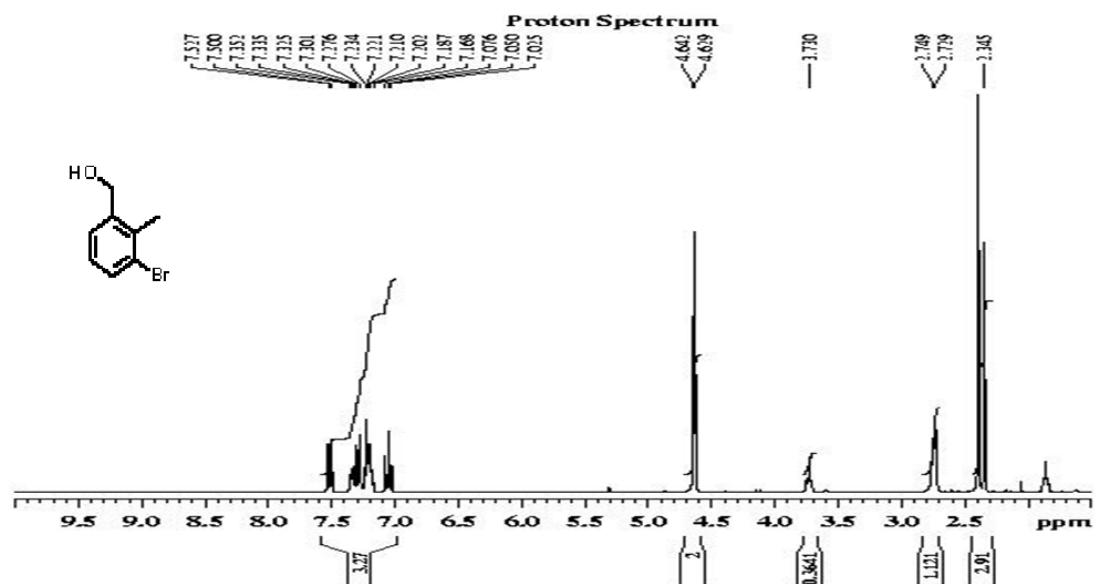


Compound BF090712D

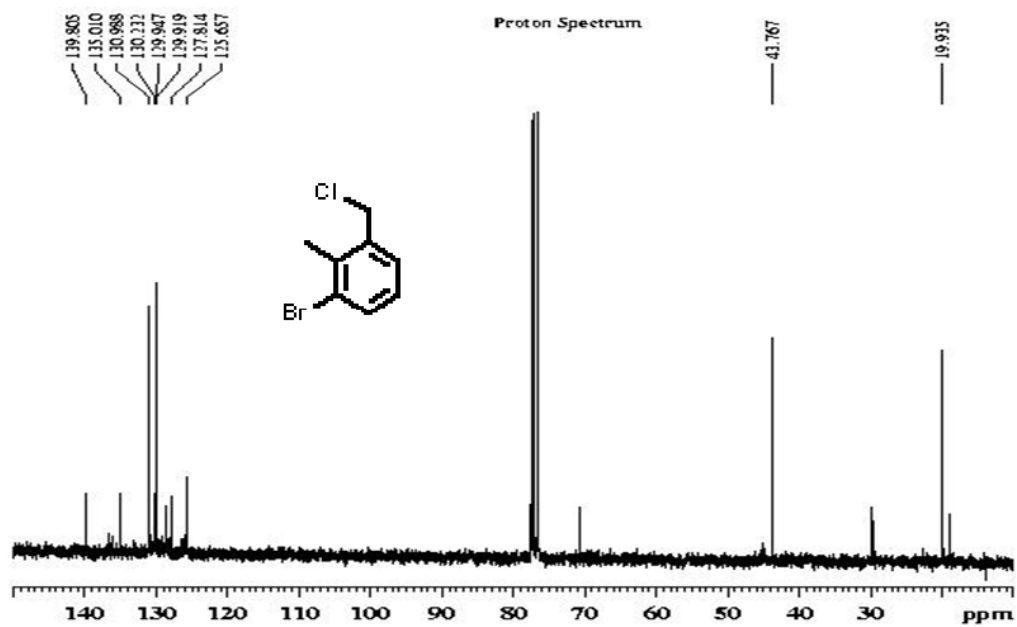
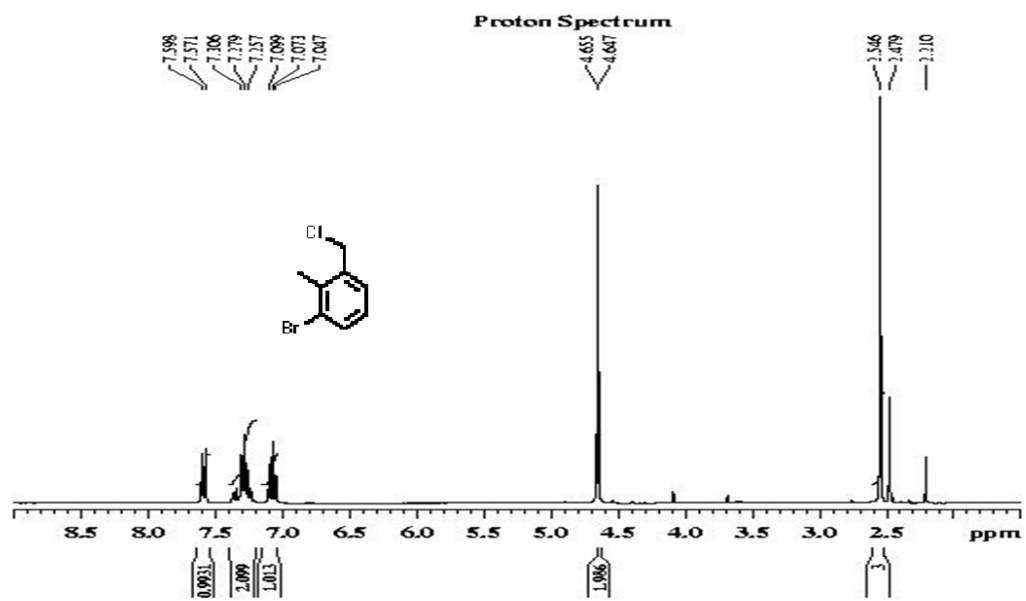




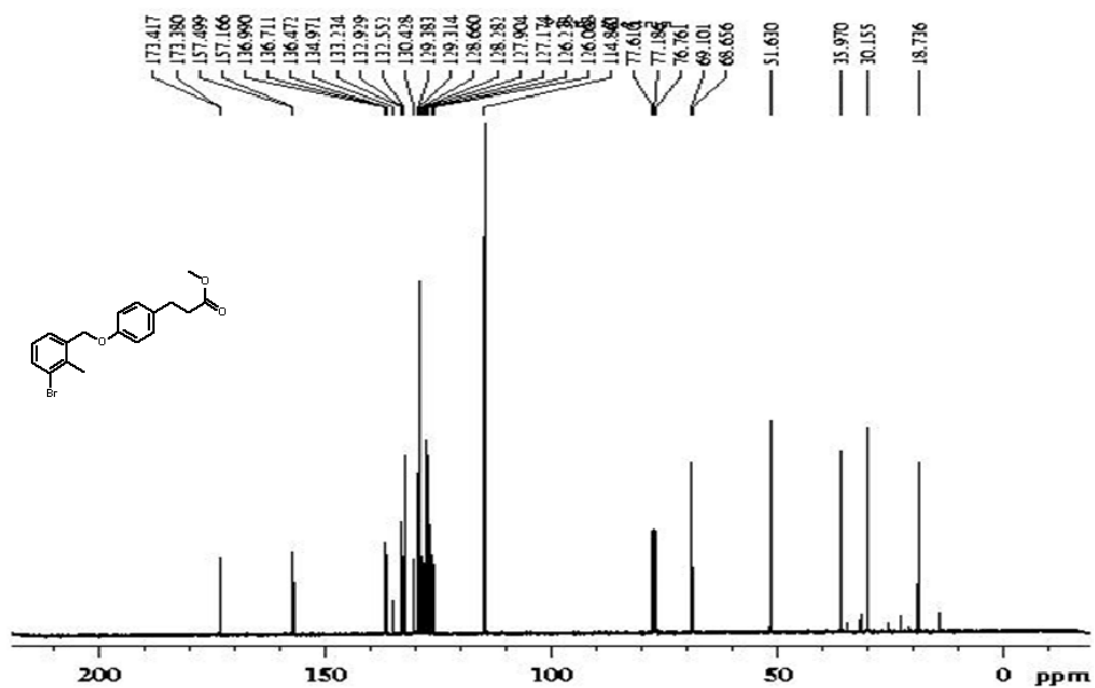
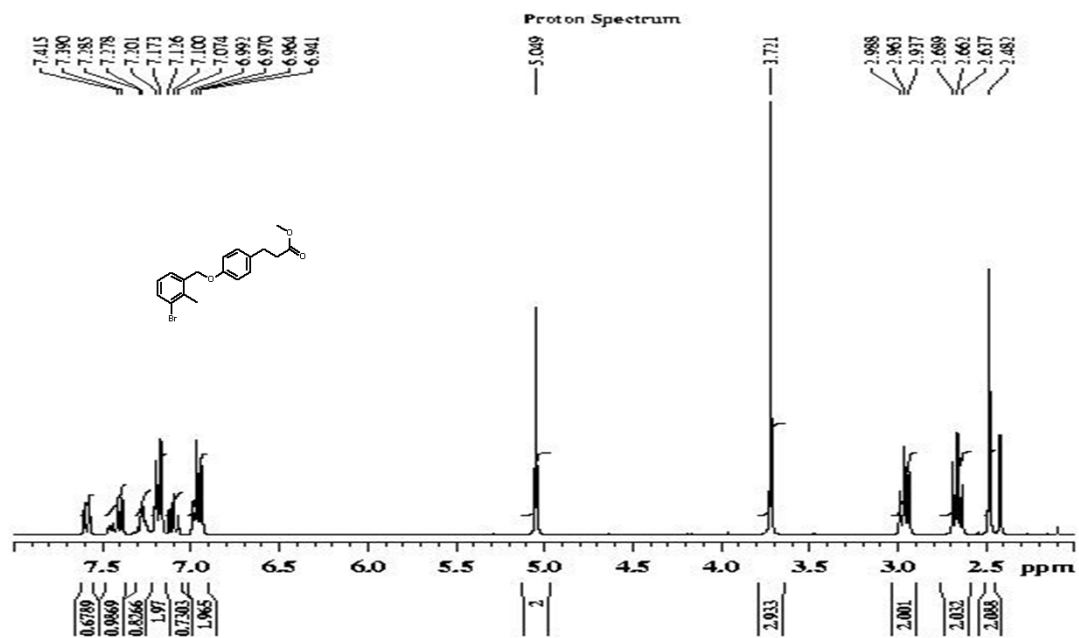
Compound 2.2



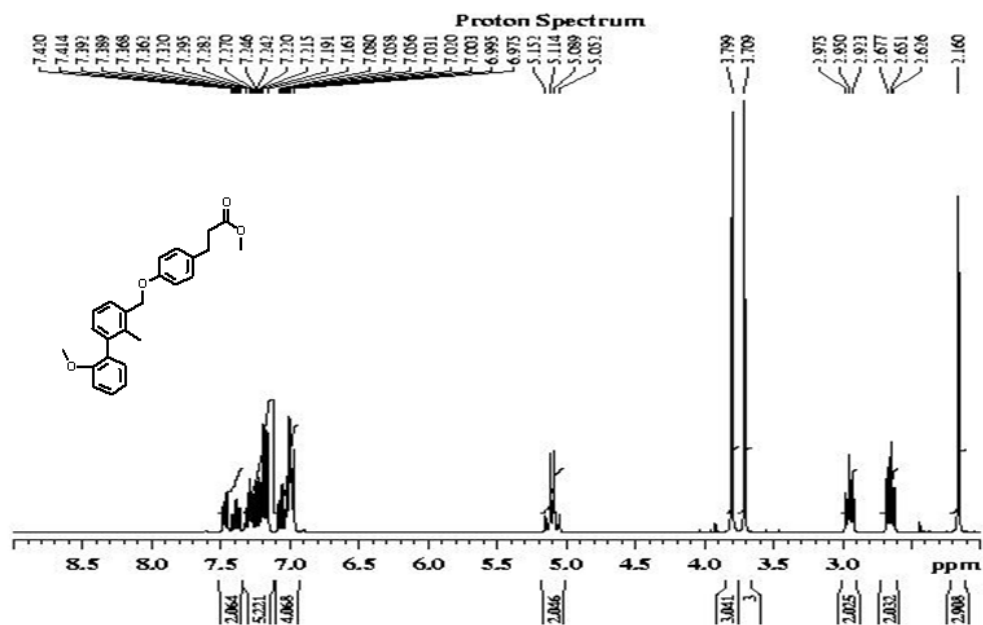
Compound 2.3.

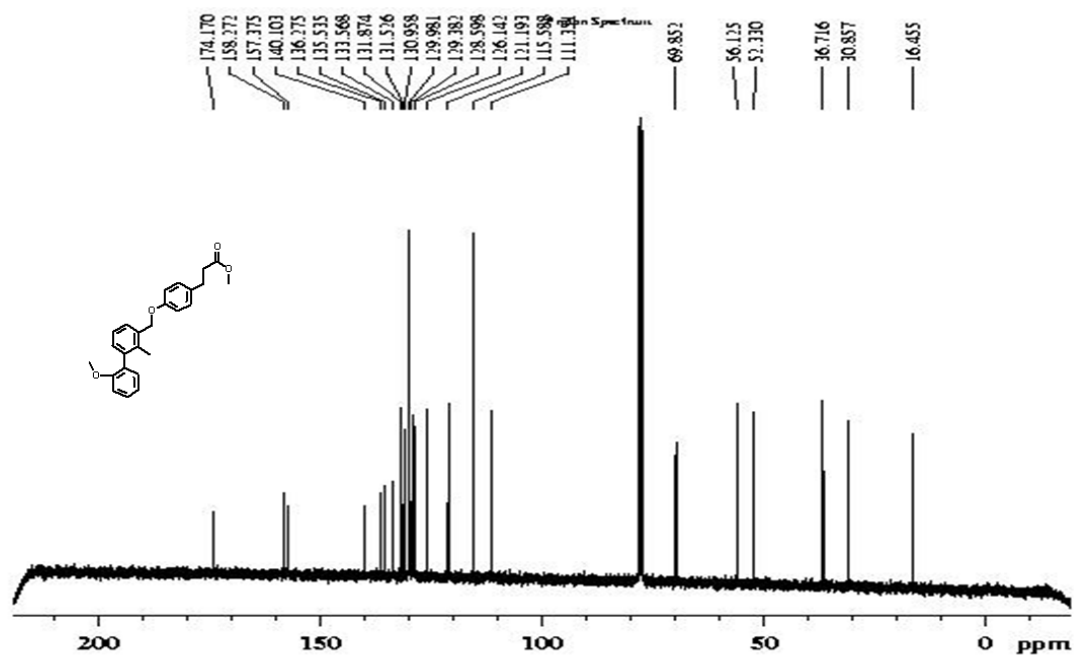


Compound BF050813G



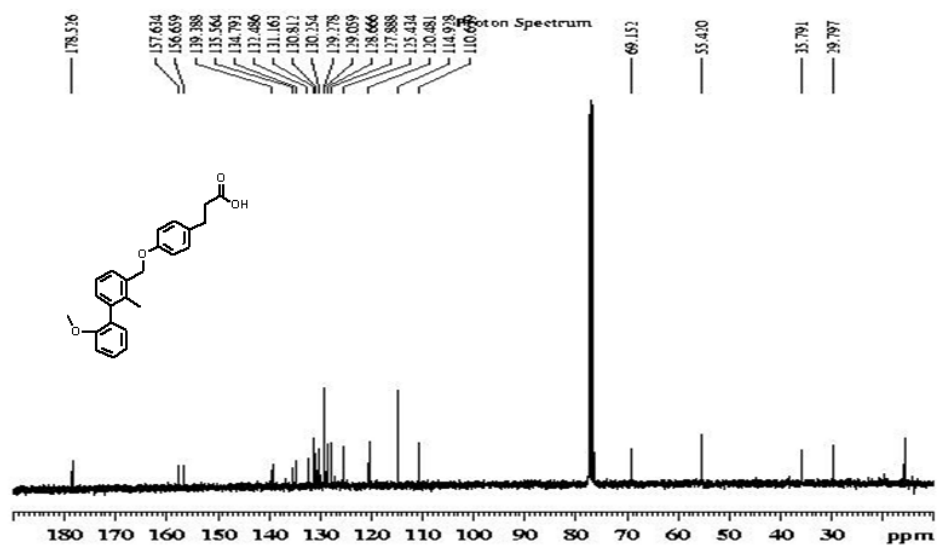
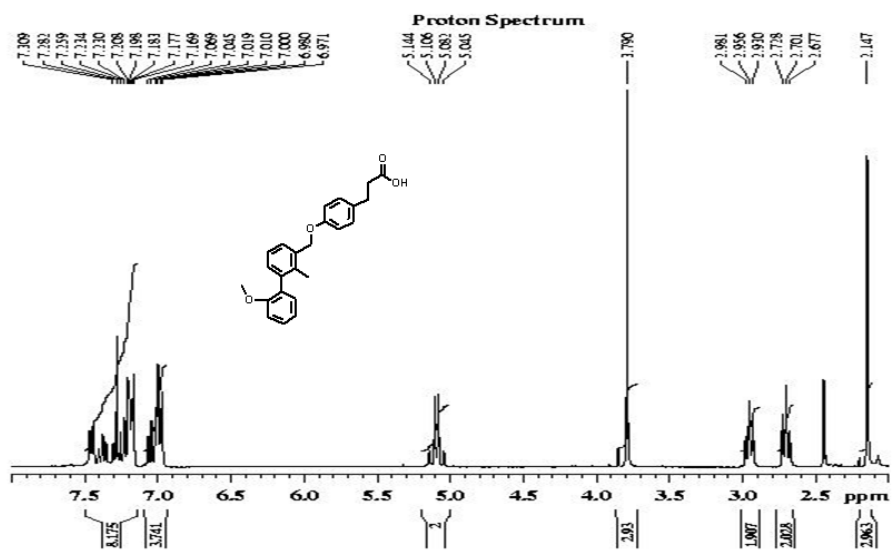
Compound BF090713B



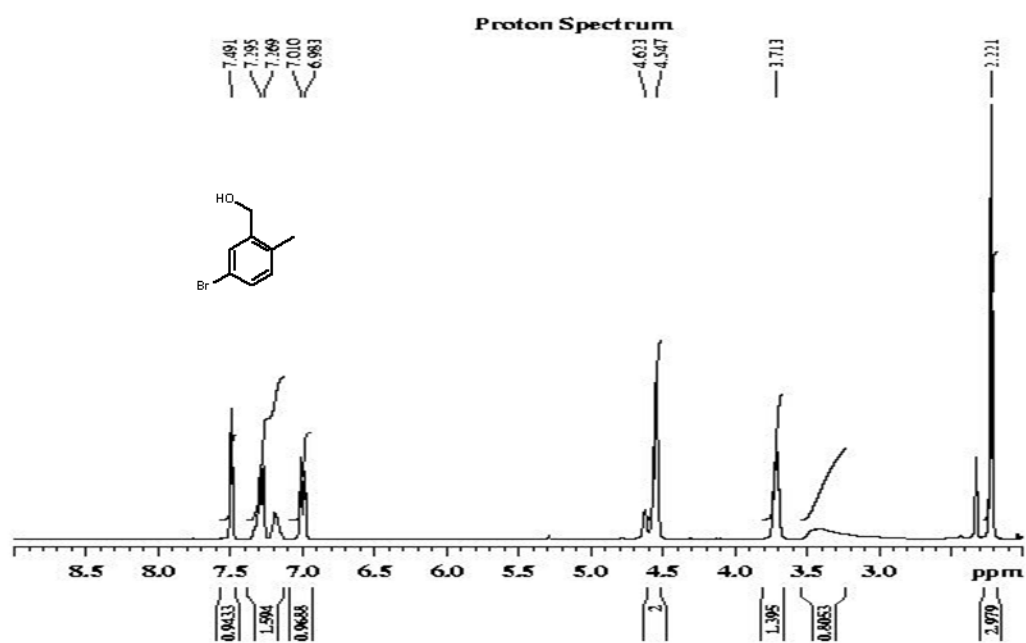


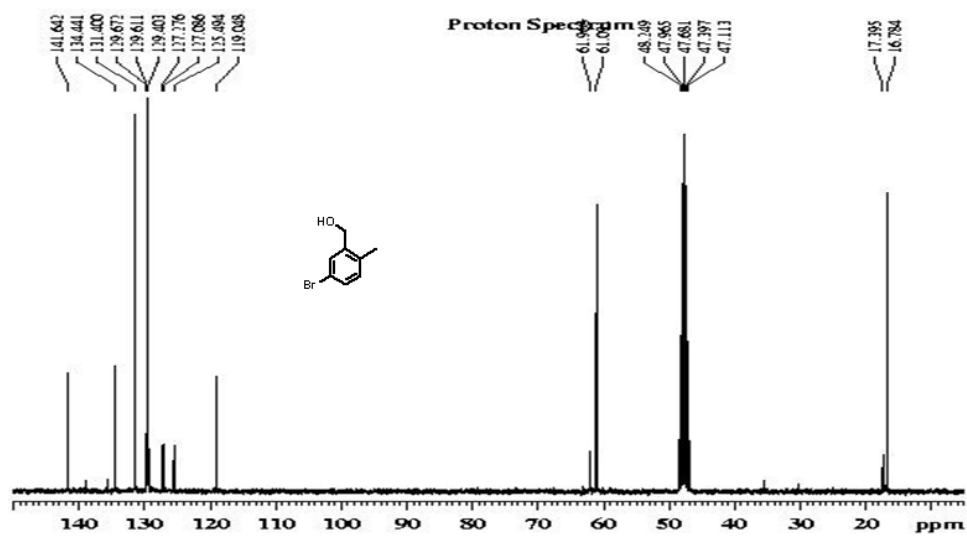
Compound

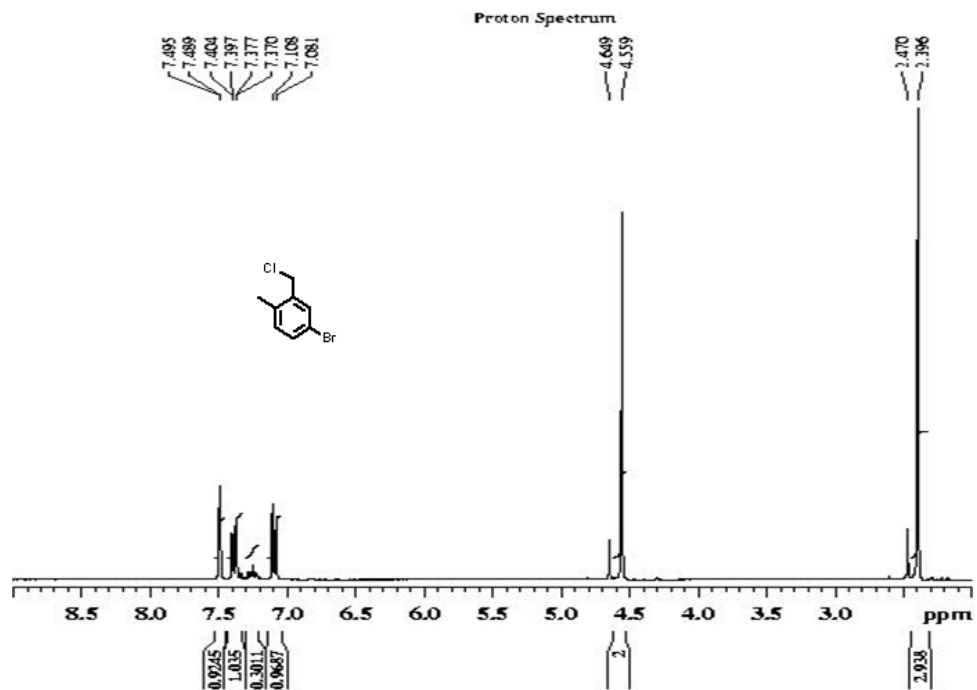
BF090713B1

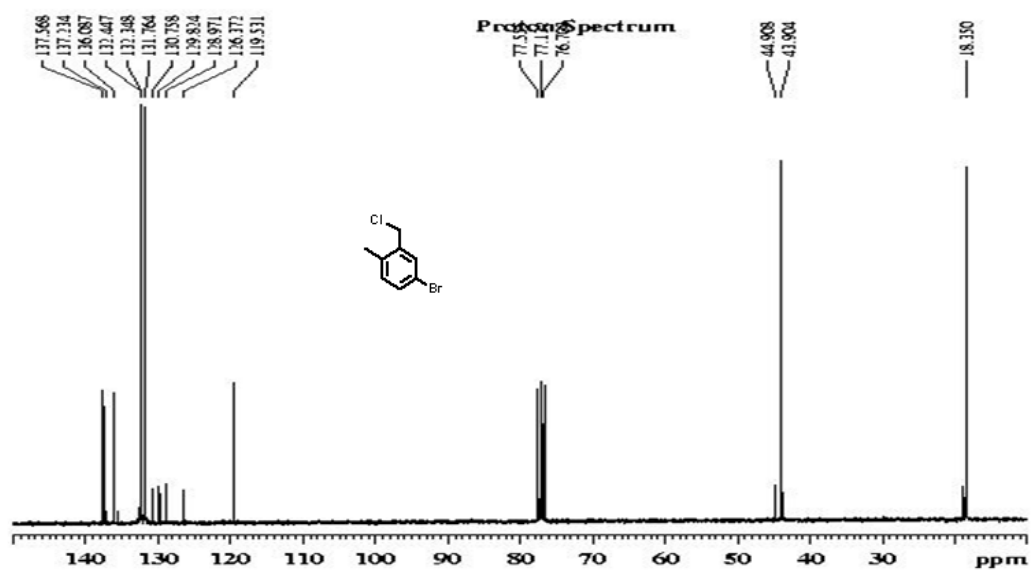


Compound 3.2

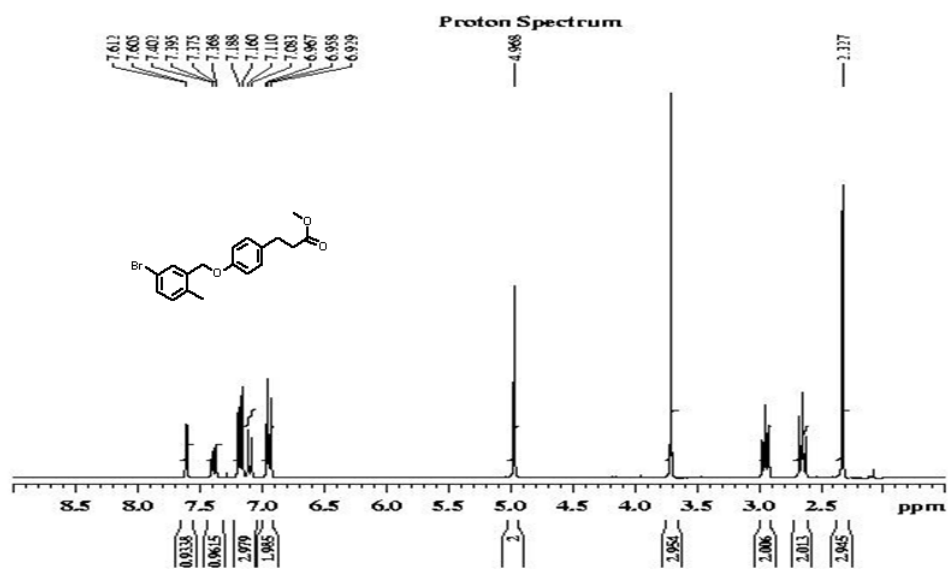


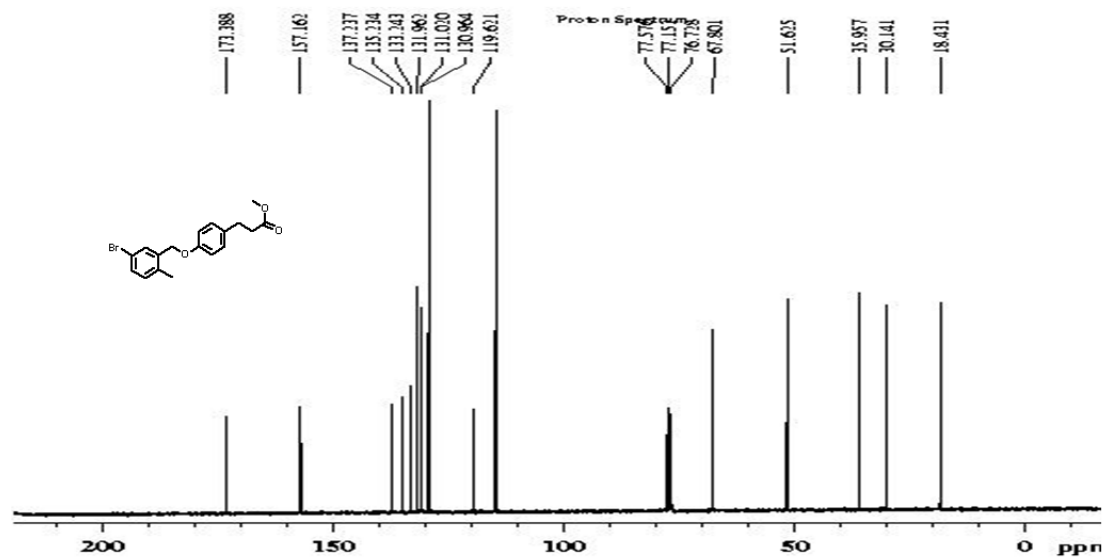
**Compound 3.3**



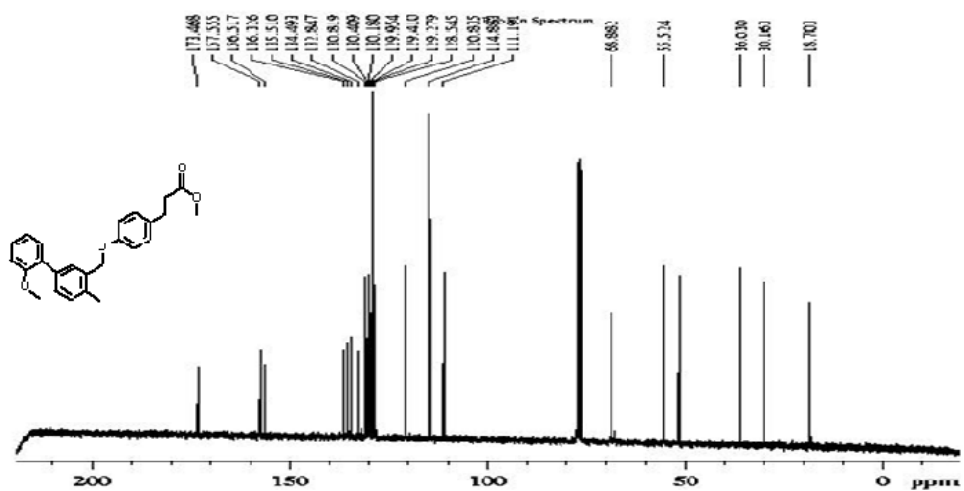
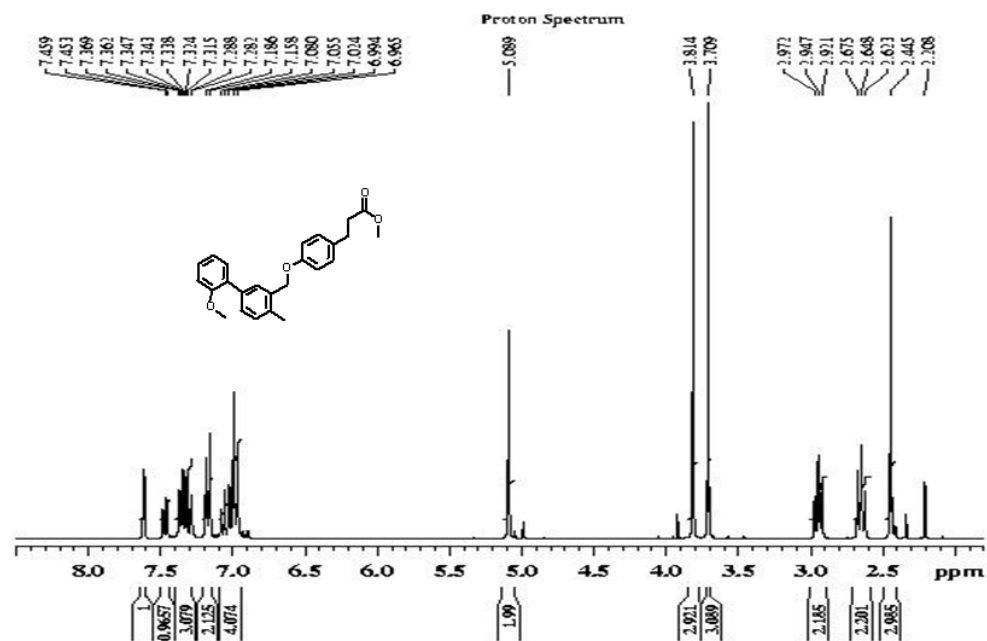


Compound BF060813H

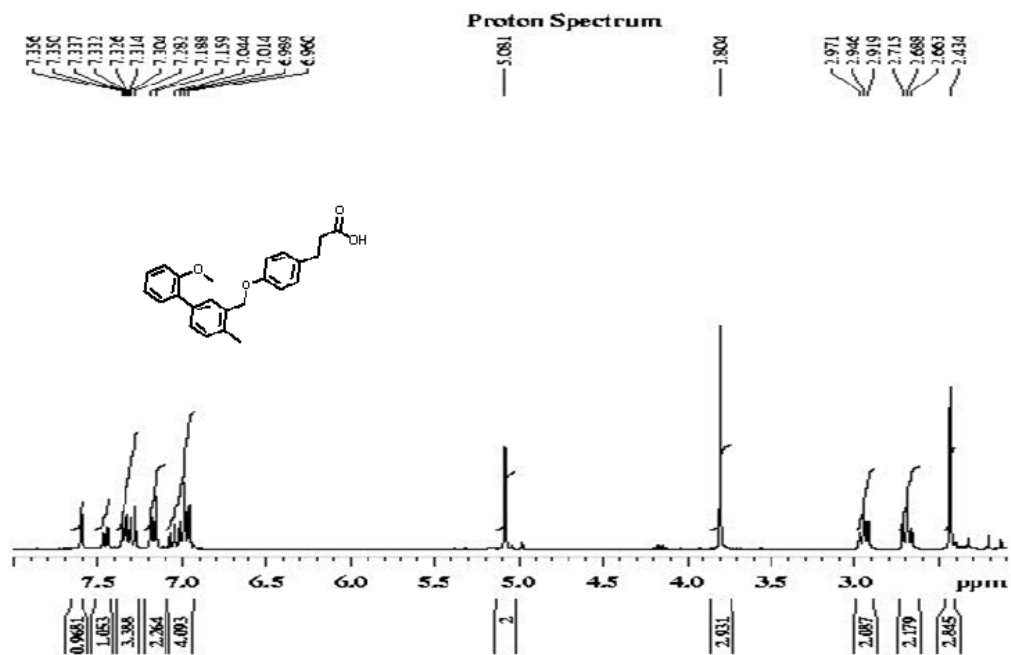


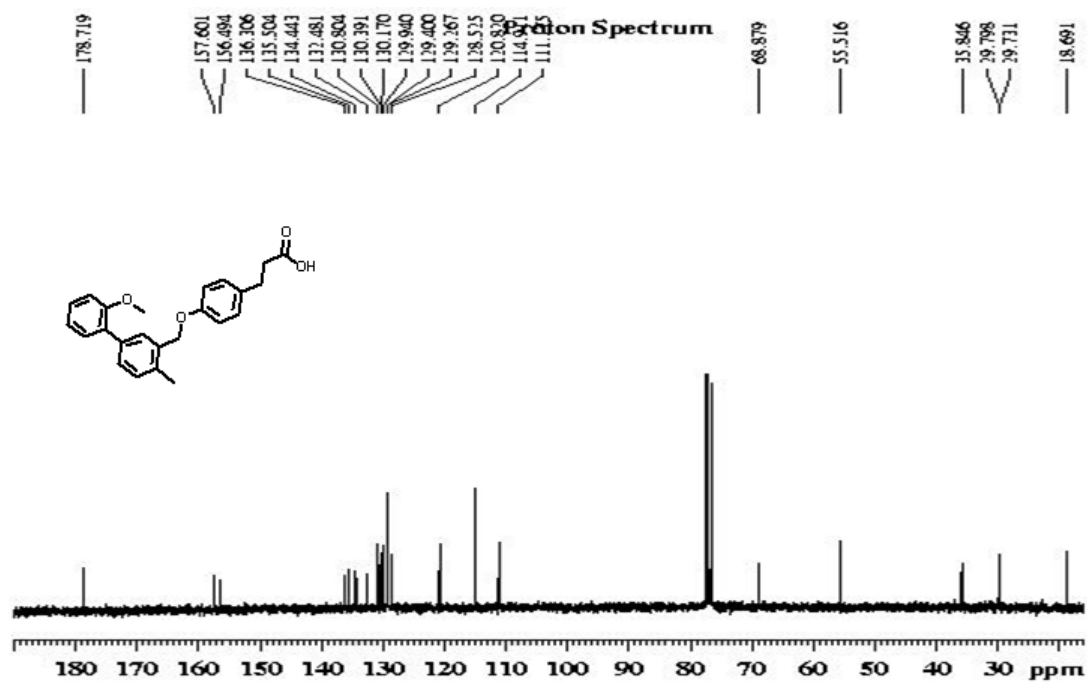


Compound BF090813A



Compound BF090813A1





CHAPTER VIII

References

- [1] P.W. Jurutka, G.K. Whitfield, J.C. Hsieh, P.D. Thompson, C.A. Haussler, M.R. Haussler (2001) Molecular nature of the vitamin D receptor and its role in regulation of gene expression. *Rev Endocr Metab Disord* 2:203-216.
- [2] S. Yamada, M. Shimizu, K. Yamamoto (2003) Vitamin D receptor. *Endocr Dev* 6:50-63.
- [3] P.L. Michal Pawlak, and Bart Staels (2012) General molecular biology and architecture of nuclear receptors. *Med Chem.* 486–504.
- [4] M.F. Holick, H.K. Schnoes, H.F. DeLuca, T. Suda, R.J. Cousins (1971) Isolation and identification of 1,25-dihydroxycholecalciferol. A metabolite of vitamin D active in intestine. *Biochemistry-U S A* 10:2799-2804.
- [5] J.A. MacLaughlin, R.R. Anderson, M.F. Holick (1982) Spectral character of sunlight modulates photosynthesis of previtamin D₃ and its photoisomers in human skin. *Science* 216:1001-1003.
- [6] J.W. Blunt, Y. Tanaka, H.F. DeLuca (1968) The biological activity of 25-hydroxycholecalciferol, a metabolite of vitamin D₃. *Proc Natl Acad Sci U S A* 61:717-718.

- [7] P.F. Brumbaugh, and Haussler, M. R (1974) 1 Alpha,25-dihydroxycholecalciferol receptors in intestine. I. Association of 1 alpha,25-dihydroxycholecalciferol with intestinal mucosa chromatin. *J Biol Chem* 1251-1257.
- [8] R.P. Esvelt, Schnoes, H. K., and DeLuca, H. F. (1979) Isolation and characterization of 1 alpha-hydroxy-23-carboxytetranorvitamin D: a major metabolite of 1,25-dihydroxyvitamin D₃. *Biochemistry-Us* 3977-3983.
- [9] R.L. Horst, Reinhardt, T. A., Ramberg, C. F., Koszewski, N. J., and Napoli, J. L. (1986) 24-Hydroxylation of 1,25-dihydroxyergocalciferol. An unambiguous deactivation process. *J Biol Chem* 9250-9256.
- [10] A. Toell, Polly, P., and Carlberg, C. (2000) All natural DR3-type vitamin D response elements show a similar functionality in vitro. *The Biochemical journal* 301-309.
- [11] D.J. Mangelsdorf, R.M. Evans (1995) The R_{xr} Heterodimers and Orphan Receptors. *Cell* 83:841-850.
- [12] J.Y. Kim, Y.L. Son, Y.C. Lee (2009) Involvement of SMRT corepressor in transcriptional repression by the vitamin D receptor. *Mol Endocrinol* 23:251-264.
- [13] H. Masuyama, C.M. Brownfield, R. St-Arnaud, P.N. MacDonald (1997) Evidence for ligand-dependent intramolecular folding of the AF-2 domain in vitamin D receptor-activated transcription and coactivator interaction. *Mol Endocrinol* 11:1507-1517.
- [14] H. Hong, K. Kohli, M.J. Garabedian, M.R. Stallcup (1997) GRIP1, a transcriptional coactivator for the AF-2 transactivation domain of steroid, thyroid, retinoid, and vitamin D receptors. *Mol Cell Biol* 17:2735-2744.

- [15] H. Li, P.J. Gomes, J.D. Chen (1997) RAC3, a steroid/nuclear receptor-associated coactivator that is related to SRC-1 and TIF2. *Proc Natl Acad Sci U S A* 94:8479-8484.
- [16] Y. Mita, K. Dodo, T. Noguchi-Yachide, H. Miyachi, M. Makishima, Y. Hashimoto, M. Ishikawa (2010) LXXLL peptide mimetics as inhibitors of the interaction of vitamin D receptor with coactivators. *Bioorg Med Chem Lett* 20:1712-1717.
- [17] Y. Mita, K. Dodo, T. Noguchi-Yachide, Y. Hashimoto, M. Ishikawa (2013) Structure-activity relationship of benzodiazepine derivatives as LXXLL peptide mimetics that inhibit the interaction of vitamin D receptor with coactivators. *Bioorg Med Chem* 21:993-1005.
- [18] P.S. Sidhu, N. Nassif, M.M. McCallum, K. Teske, B. Feleke, N.Y. Yuan, P. Nandhikonda, J.M. Cook, R.K. Singh, D.D. Bikle, L.A. Arnold (2014) Development of Novel Vitamin D Receptor-Coactivator Inhibitors. *Acs Med Chem Lett* 5:199-204.
- [19] P. Nandhikonda, W.Z. Lynt, M.M. McCallum, T. Ara, A.M. Baranowski, N.Y. Yuan, D. Pearson, D.D. Bikle, R.K. Guy, L.A. Arnold (2012) Discovery of the First Irreversible Small Molecule Inhibitors of the Interaction between the Vitamin D Receptor and Coactivators. *Journal of Medicinal Chemistry* 55:4640-4651.
- [20] D. Miura, K. Manabe, K. Ozono, M. Saito, Q. Gao, A.W. Norman, S. Ishizuka (1999) Antagonistic action of novel 1 α ,25-dihydroxyvitamin D₃-26, 23-lactone analogs on differentiation of human leukemia cells (HL-60) induced by 1 α ,25-dihydroxyvitamin D₃. *J Biol Chem* 274:16392-16399.

- [21] Y. Bury, A. Steinmeyer, C. Carlberg (2000) Structure activity relationship of carboxylic ester antagonists of the vitamin D(3) receptor. *Mol Pharmacol* 58:1067-1074.
- [22] M. Igarashi, N. Yoshimoto, K. Yamamoto, M. Shimizu, M. Ishizawa, M. Makishima, H.F. DeLuca, S. Yamada (2007) Identification of a highly potent vitamin D receptor antagonist: (25S)-26-adamantyl-25-hydroxy-2-methylene-22,23-didehydro-19,27-dinor-20-epi-vitamin D₃ (ADMI3). *Arch Biochem Biophys* 460:240-253.
- [23] Y. Inaba, N. Yoshimoto, Y. Sakamaki, M. Nakabayashi, T. Ikura, H. Tamamura, N. Ito, M. Shimizu, K. Yamamoto (2009) A new class of vitamin D analogues that induce structural rearrangement of the ligand-binding pocket of the receptor. *J Med Chem* 52:1438-1449.
- [24] P. Nandhikonda, A. Yasgar, A.M. Baranowski, P.S. Sidhu, M.M. McCallum, A.J. Pawlak, K. Teske, B. Feleke, N.Y. Yuan, C. Kevin, D.D. Bikle, S.D. Ayers, P. Webb, G. Rai, A. Simeonov, A. Jadhav, D. Maloney, L.A. Arnold (2003) GW0742 interacts weakly with multiple nuclear receptors, including the vitamin D receptor. *Biochemistry-US* 4193-4203.
- [25] M.L. Sznajdman, C.D. Haffner, P.R. Maloney, A. Fivush, E. Chao, D. Goreham, M.L. Sierra, C. LeGrumelec, H.E. Xu, V.G. Montana, M.H. Lambert, T.M. Willson, W.R. Oliver, Jr., D.D. Sternbach (2013) Novel selective small molecule agonists for peroxisome proliferator-activated receptor delta (PPARdelta)--synthesis and biological activity. *Bioorg Med Chem Lett* 1517-1521.

- [26] M.J. Zarzuelo, Jimenez, R., Galindo, P., Sanchez, M., Nieto, A., Romero, M., Quintela, A. M., Lopez-Sepulveda, R., Gomez-Guzman, M., Bailon, E., Rodriguez-Gomez, I., Zarzuelo, A., Galvez, J., Tamargo, J., Perez-Vizcaino, F., and Duarte, J. (2011) proliferator-activated receptor-beta activation in spontaneously hypertensive rats, *Hypertension*. *Hypertension* 733-743.
- [27] Y. Matsushita, Ogawa, D., Wada, J., Yamamoto, N., Shikata, K., Sato, C., Tachibana, H., Toyota, N., and Makino, H. (2011) Activation of peroxisome proliferator-activated receptor delta inhibits streptozotocin-induced diabetic nephropathy through anti-inflammatory mechanisms in mice. *Free Radic Biol Med* 960-968.
- [28] P. Sertznig, Dunlop, T., Seifert, M., Tilgen, W., and Reichrath, J. (2009) Cross-talk between vitamin D receptor (VDR)- and peroxisome proliferator-activated receptor (PPAR)-signaling in melanoma cells. *Anticancer* 3647-3658.
- [29] A.M. Rossi, C.W. Taylor (2011) Analysis of protein-ligand interactions by fluorescence polarization. *Nature protocols* 365-387.
- [30] W.J. Checovich, R.E. Bolger, T. Burke (1995) Fluorescence polarization--a new tool for cell and molecular biology. *Nature* 254-256.
- [31] *Transient Kinetics & Spectroscopy*, in, 2014.
- [32] W.B. Dandliker, M.L. Hsu, J. Levin, B.R. Rao (1981) Equilibrium and kinetic inhibition assays based upon fluorescence polarization. *Methods in enzymology* 3-28.

- [33] A. Teichert, L.A. Arnold, S. Otieno, Y. Oda, I. Augustinaite, T.R. Geistlinger, R.W. Kriwacki, R.K. Guy, D.D. Bikle (2009) Quantification of the vitamin D receptor-coregulator interaction. *Biochemistry* 48:1454-1461.
- [34] W. Hakamata, Y. Sato, H. Okuda, S. Honzawa, N. Saito, S. Kishimoto, A. Yamashita, T. Sugiura, A. Kittaka, M. Kurihara (2008) (2S,2'R)-analogue of LG190178 is a major active isomer. *Bioorganic & medicinal chemistry letters* 120-123.
- [35] J.W.P. David Feldman, John S. Adams, *Vitamin D*, 3rd ed., Elsevier Inc., 2011.
- [36] in: *Isogen-lifescience*.
- [37] H. Fraga, Fernandes, D., Novotny, J., Fontes, R., and da Silva, J. C. G. (2006) Firefly luciferase produces hydrogen peroxide as a coproduct in dehydroluciferyl adenylate formation. *Chembiochem* 929-935.
- [38] P.J. Brown, L.W. Stuart, K.P. Hurley, M.C. Lewis, D.A. Winegar, J.G. Wilson, W.O. Wilkinson, O.R. Ittoop, T.M. Willson (2001) Identification of a subtype selective human PPAR alpha agonist through parallel-array synthesis. *Bioorganic & Medicinal Chemistry Letters* 11:1225-1227.